이학박사학위논문

Optimizing the Electrical Properties of CVD Graphene by Substrate and Doping Control

화학기상증착 그래핀의 전기적 특성 최적화 연구

2017 년 8 월

서울대학교 대학원
화학부 물리화학 전공

조 인 수

화학기상증착 그래핀의 전기적 특성 최적화 연구

Optimizing the Electrical Properties of CVD Graphene by Substrate and Doping Control

지도교수: 홍 병 희

이 논문을 이학박사 학위논문으로 제출함

2017년 8월

서울대학교 대학원

화학부 물리화학전공

조 인 수

조인수의 이학박사 학위논문을 인준함

2017년 8월

위 원 장	장두전	(인)
부위원장	홍병희	(인)
위 원	민달희	(인)
위 원	조성표	(인)
위 원	박수범	(인)

A Ph. D. Dissertation

Optimizing the Electrical Properties of CVD Graphene by Substrate and Doping Control

Supervisor: Professor Byung Hee Hong

Major: Physical Chemistry

By Insu Jo

Department of Chemistry

Graduate School of Seoul National University

2017

Abstract

Optimizing the Electrical Properties of CVD Graphene by Substrate and Doping Control

Insu Jo
Department of Chemistry
The Graduate School Seoul National Univeristy

After the first artificially-isolated single-atom-thick material, which is graphene, the new era of two-dimensional materials has begun. With its extraordinary physical and chemical properties, graphene has drawn considerable attention as a subject of the fundamental research by condensed matter physicists. Thereafter, the realization of large scale graphene synthesis on catalytic substrates, such as Ni, Fe, and especially Cu, by chemical vapor deposition (CVD) makes researchers in numerous fields rush into graphene study.

Though large-scale graphene films synthesized by the CVD method shows tremendous potential of applications for transparent electrodes with high electrical, optical properties and mechanical stability, the CVD-grown graphene films still have higher sheet resistance, compared to the exfoliated graphene. One of the limiting factors to degrade graphene quality is polycrystallinity and grain boundary of graphene, which originated from the randomly oriented nucleation and growth of graphene islands.

Another factor is the ruga morphology of graphene, which is induced by the different thermal expansion coefficient between graphene and catalyst. The cooling down process makes catalyst

surface corrugated and it leads to quasi periodic nanoripple arrays of graphene after graphene transfer onto target substrates. The rippled graphene gives rise to flexural phonon scattering, which play a limiting role in charge mobility and sheet resistance.

The present thesis addresses the synthesis of graphene by CVD on copper, which has become the most popular catalyst for graphene growth. A significant study on the graphene growth and property control is reported in the present thesis.

This dissertation provides the details of my work on all projects related to synthesize and characterization of the graphene synthesis by CVD on copper and its application for field effect transistor. Especially, we will discuss the improvement of the sheet resistance of graphene by controlling synthesis condition. We also controlled the work function of graphene films via vapor phase doping process.

First, tension-controlled graphene growth is presented herein. The methods for optimizing the crystalline orientations of Cu foils by tension control are explained in detail. In addition, the optimized Cu foils allow the growth of larger single-crystalline graphene with higher charge carrier mobility.

Second, we demonstrated tuning the cooling rate can control the electrical properties of CVD-grown graphene. A higher cooling rate gives rise to large suspended graphene formation, which in turn results in reduced ripple density and its heights after transfer onto SiO_2/Si substrates.

Finally, an improved graphene doping method is also described. we have investigated the effect of the dopant structure and number

of amines group in dopant. The doping concentration was stronger as increasing amino group in linear ethylene amine structure. However, the branched structure showed weaker doping, although it has the most amino functional groups in the series of ethylene amine dopants.

In conclusion, we believe that our findings will provide crucial ideas to design a system for the CVD growth of high-quality graphene films on roll-to-roll Cu foils which would be of great importance for the continuous mass-production of graphene films for practical applications in the future.

Keyword : chemical vapor deposition(CVD), Cu foil, graphene, texture, ripple, wrinkle, doping.

Student Number : 2012-23052

Table of Contents

List of Figures

Chapter 1.

Cu subsrates and its height profile along the line direction. (e) Sketch map showing the positions of wrinkles and ripples with substrate states. [Adapted from Ref. 12]

Figure 1.9. Wrinkles formation in CVD process (a) An AFM image of a hexagonal graphene island on Cu surface. (b) Schematic diagram showing the top view of a hexagonal graphene flake on Cu(110). (c) Schematic diagrams showing the effect of thermal expansion mismatch on the formation of graphene ripples. [Adapted from Ref. 13]

Figure 1.10. AFM images of (a) Cu surface and (b) CVD graphene on SiO_2. (c) AFM line scans reveal nanoripple arrays which are closely correlated with the Cu terraces. T-dependent sublinear conductivity for nanoripple arrays (d) parallel and (e) perpendicular configuration. [Adapted from Ref. 14]

Figure 1.11. (a) A schematic representation of the nitrogen doped graphene. (b) A schematic of the structure of graphene oxide and its reaction with ammonia through thermal annealing. [Adapted from Ref. 15]

Figure 1.12. Schematic band structures of graphene. (a)Band structure of pristine graphene with zero bandgap. Band structures of (b) p-type and (c) n-type graphene with the bandgap. [Adapted from Ref. 16]

Figure 1.13. (a) The scheme of the graphene field effect transistor device. (b) The energy diagram shows a potential barrier with height V and the position of the Fermi level with respect to the touching point of the valence and the conduction bands. [Adapted from Ref.

16] (c) Schematic diagram of the vapor-phase doping process.

Chapter 2.

Figure 2.1. The methods to obtain Cu(111) substrates. Cu deposition on (a) sapphire and (b) SiO_2 wafer. Cu(111) was obtained by prolonged annealing. [Adapted from Ref. 10, 12, and 13]

Figure 2.2. Surface orientation of CVD processed Cu foil at different temperatures. (a) 800, (b) 900, and (c) 1000 °C.

Figure 2.3. (a-c) Photographs of a horizontal-vertical switchable CVD system and a holding jig. (d, e) Schematic illustrations of horizontally and vertically loaded Cu foils without additional tension, respectively. (f) A schematic illustration of a vertically loaded Cu foil with tension applied by a weight. (g) An illustration of the in situ switchable horizontal-vertical CVD system, which provides identical growth conditions except the vertical tension by gravitation or additional weights applied to Cu foils.

Figure 2.4. Grain boundary(GB) identification through diffraction series on a graphene sheet. (adapted from reference [22])

Figure 2.5. Optical microscope image of graphene field effect transistor, scale bar = 50 mm.

Figure 2.6. (a-c) EBSD images of annealed and graphene-grown Cu surface with horizontal/vertical geometry with/without tension control. (d) XRD spectra of annealed and graphene-grown Cu surface with and without tension control. The 2Θ measured from 30° to 80°

shows the three intense peaks at 43°, 50°, and 74°, which are assigned to Bragg reflections from the surface of Cu (111), (100), and (110), respectively. (e) SEM and EBSD images of graphene islands of Cu, indicating that the recrystallization of Cu surface can be promoted by graphene in the case of tension-controlled growth.

Figure 2.7. SEM and EBSD images obtained from 3 different batches at the same position on the graphene-grown Cu foils that are vertically loaded with controlled tension, indicating that the single-crystallization into Cu is reproducible.

Figure 2.8. SEM and EBSD images of partially grown graphene islands on a vertically loaded Cu foil with controlled tension. The Cu surface underneath graphene islands tends to be reoriented by the interaction with graphene lattice at the interface.

Figure 2.9. Grain boundary analyses of graphene by scanning diffraction mapping in TEM, indicating that the graphene from vertically loaded Cu with tension (c) shows the larger domain sizes than the cases of the horizontally loaded Cu (a) and the vertically loaded Cu without additional tension (b).

Figure 2.10. (a) FWHM(2D) and I(2D)/I(G) values for the Raman spectra (excitation λ = 514 nm) of the horizontal, vertical, and vertical Cu with tension, corresponding to Fig. 1d-e, respectively.). Raman spectroscopy was performed using a 514 nm laser (b) Field-effect transistor (FET) characteristics of graphene grown on the horizontal (red), vertical (green), and vertical Cu with tension (blue), showing the highest conductance and carrier mobility of the graphene grown on Cu (111).

Chapter 3.

Chapter 4.

List of Figures

Chapter 1.

Chapter 4.

Chapter 1. Introduction

1.1. General introduction

Graphene is an allotrope of carbon and one-atom thick planar sheet of carbon atoms that are densely packed in a honeycomb crystal lattice. (as shown in Figure 1.1)

Since the first segregation and investigation of single layer graphene using a mechanical exfoliation method, enormous studies have been investigated. The fundamental studies of graphene show that graphene has extraordinary mechanical strength, thermal conductivity, electrical and optical properties.(as described in Table 1.1) Due to these properties, graphene has drawn considerable attention by its potential for advanced technological applications such as flexible transparent conductors, integrated circuit elements, high-frequency transistors, supercapacitors, battery electrodes, membranes, passivation layers and so on.

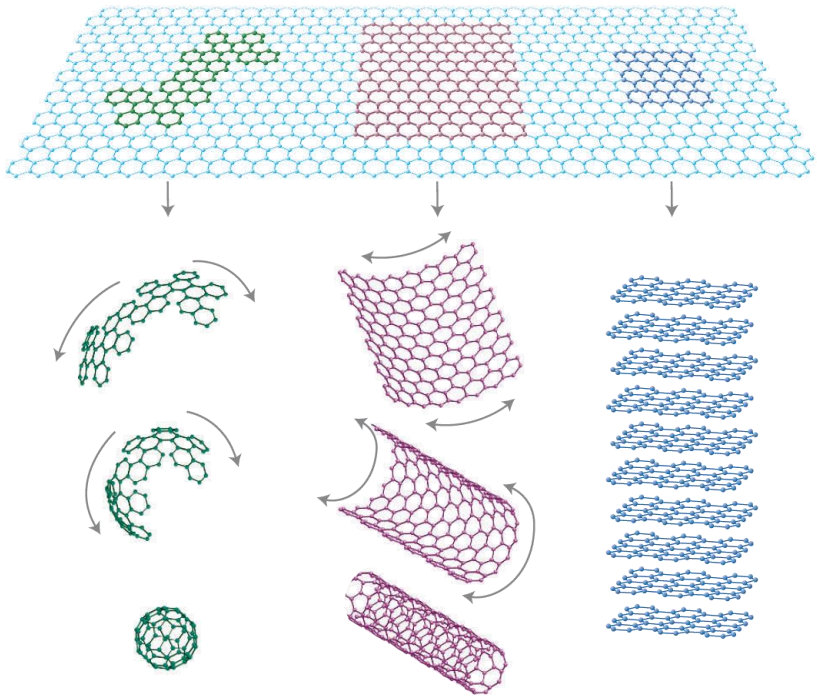

Figure 1.1. graphene is a 2D building materials of all other dimensionalities. It can be wrapped up into fullerene, rolled into carbon nanotubes or stacked into graphite. [Adapted from Ref. 1]

Table 1.1. Comparison the properties of graphene with other materials.

	ITO	CNT	Graphene
Mechanical (GPa)	119	500	1020
Thickness (nm)	100~200	7	0.34 (1 layer)
Transmittance (%)	>90 (t=100 nm)	90 (7 nm)	97.7 (0.34 nm)
Heat Conductivity (W/m-K)	11~12	3500	5000 (sub K) 600 (300 K)
Failure stain (%)	1.4	>11	>18
Sheet Resistance (Ω/sq)	< 25 (90%)	~500 (90 %)	≈ 35 (90 %)
Mobility (cm^2/Vs)	41~46	10,000	8,000 (CVD) 10,000 (HOPG)

1.2. Graphene synthesis

1.2.1. Mechanical exfoliation

Mechanical exfoliation is a method that is accomplished by peeling off the graphene from graphite using a tape, and it is called the "scotch-tape method".[2] Due to very weak interaction energy between graphite layers, graphene layers can be peeled off onto the adhesive tape. Figure 1.2. shows micromechanical exfoliation of graphene and transferring on a target substrate. The number of graphene layers can be characterized by apparent contrast using optical microscopy, its heights using atomic force microscopy, and Raman spectroscopy.

While the exfoliation is a simple, low cost method and produces very pure single-domain graphene with nearly the ideal properties, it has one large disadvantage. The graphene from highly oriented pyrolytic graphite (HOPG) or Kish graphite can only provide micrometer- to sub-micrometer-sized graphene. Due to issues with scaling and reproducibility, a wide variety of mechanical exfoliation techniques are unsuitable for the application of graphene in electrical devices and require a large-scale synthesis method.

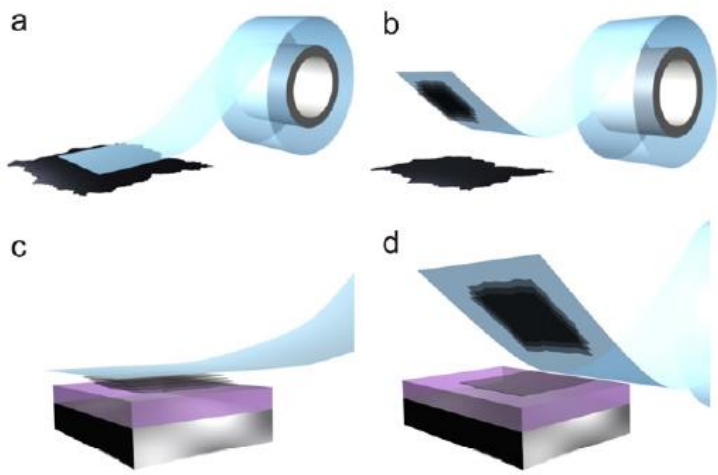

Figure 1.2 Micromechanical exfoliation of graphene. (a) Adhesive tape is pressed against a graphene. (b) Few layers of graphene are attached to the tape. (c) The tape with layers of graphene is pressed against a surface of target substrate. (d) Upon peeling off, the bottom layer is left on the substrate. [Adapted from Ref. 2]

1.2.2. Chemical exfoliation

The chemical exfoliation demonstrated the possibility of low-cost synthesis and fabrication of large-scale transparent films.(as shown in Figure 1.3) Chemical exfoliation is an exfoliation method that uses liquid phases. The interaction between graphite layers is reduced by oxidation of graphite using strong acids or oxidants. The difference between hydrophilic oxidized graphene and hydrophobic graphite crystal allows water intercalate into graphene oxide and graphite crystal. After the dispersion, oxidized graphene can be reduced with various reductants and these reduced graphene oxides can be deposited on a target substrate.[3]

However, the assembled graphene films show relatively poor electrical conductivity owing to the poor interlayer junction contact resistance and structural defects formed during the vigorous exfoliation and reduction processes. Therefore, the chemical exfoliation method has limitations, and efforts to improvement are still needed.

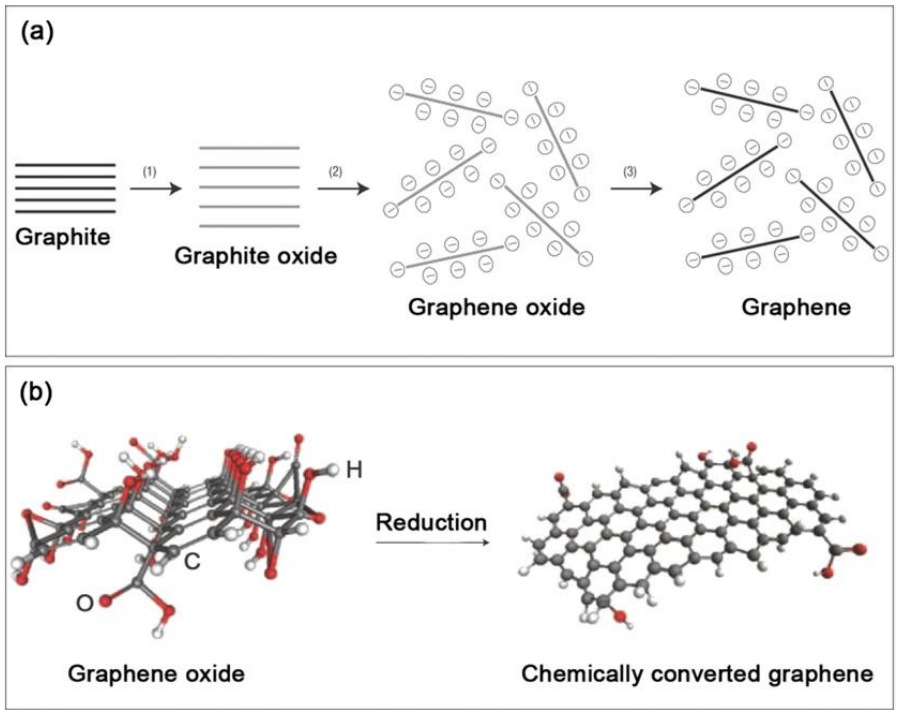

Figure 1.3. Chemical exfoliation of graphene. (a) The chemical route to the synthesis of solubilized graphene. (b) 3D molecular models of graphene oxide and reduced graphene oxide. [Adapted from Ref. 3]

1.2.3. Chemical vapor deposition (CVD)

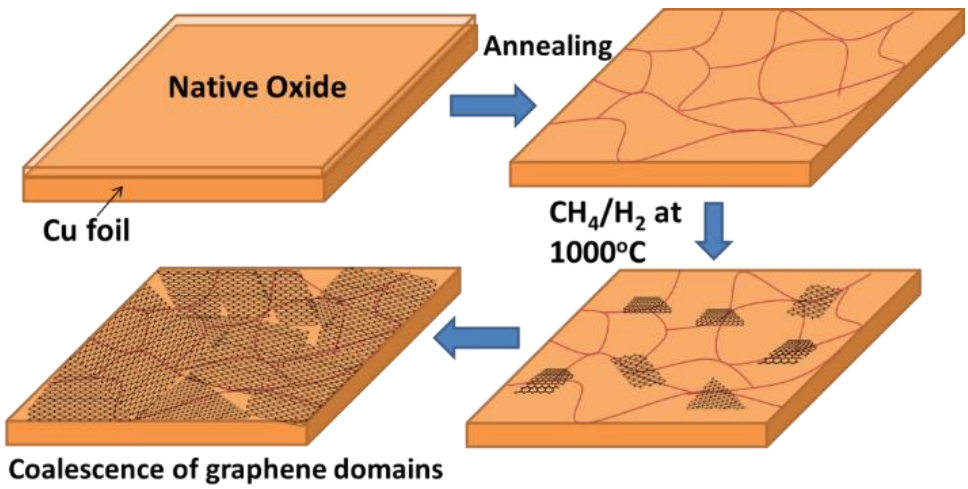

Figure 1.4. Schematic illustration of the growth mechanism of graphene on Cu substrates by CVD. [Adapted from Ref. 4]

A more recent approach for graphene synthesis, instead of the exfoliation method or graphene oxide, is chemical vapor deposition (CVD). Graphene is grown on surface of transition metal catalyst, such as Ni[5], Fe[6], Cu[4], Ir[7], and Ru[8], using hydrocarbon gas at near melting point of catalyst. Among the transition metal catalyst, due to its low carbon solubility, Cu is the most attractive catalyst for the synthesis of monolayer graphene.[4]

As shown in Figure 1.5., the CVD synthesis of graphene has several important processes. A metal catalyst, such as Cu, is put into a furnace and heated under hydrogen containing atmosphere. Carbon gas, such as methane, ethylene, and acetylene, is then flowed through the furnace with hydrogen. The hydrogen induces decomposition of carbon source into carbon atoms. Then the carbon

atoms are deposited onto the surface of the Cu through chemical adsorption and makes continuous graphene sheet on the Cu surface. After synthesis, graphene can be transferred onto target surface. For this step, undesired catalyst and graphene layer should be etched away. After transfer process, graphene properties can be tuned by doping.

Though large-scale graphene films synthesized by the CVD method shows tremendous potential of applications for transparent electrodes with high electrical, optical properties and mechanical stability, the CVD-grown graphene films still have higher sheet resistance, compared to the exfoliated graphene.

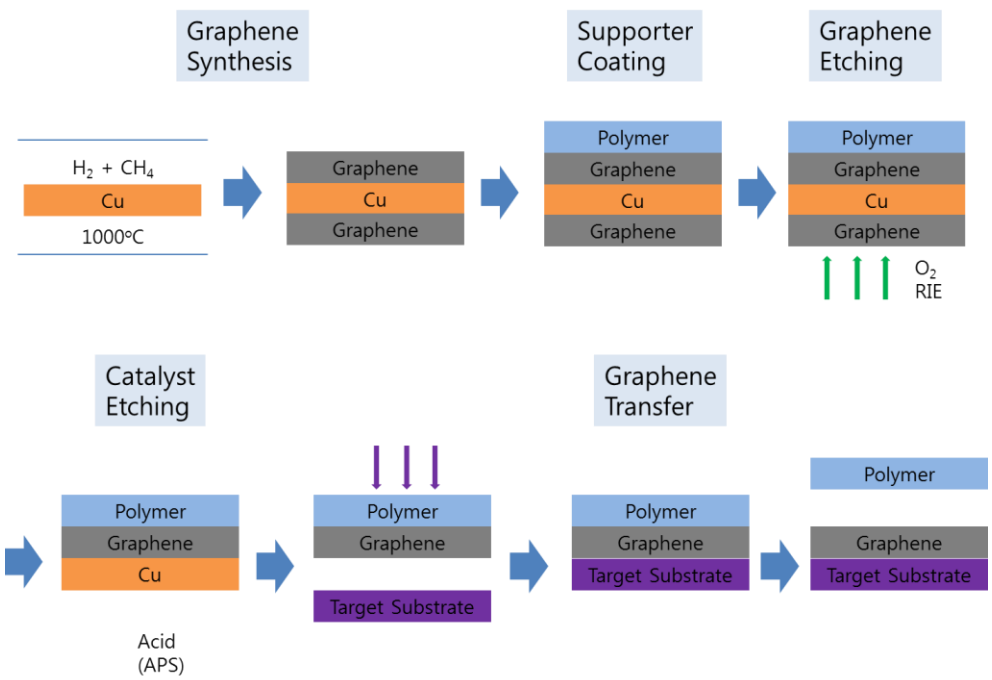

Figure 1.5. Synthesis, etching and transfer processes for the large-scale graphene films using Cu catalyst.

Figure 1.6. shows the important factors of CVD graphene fabrication process to get the high-quality graphene. Among the factors, CVD condition, metal catalyst, and doping are the most important points for the little defects and larger grain graphene, and these will be discussed in the follow sections

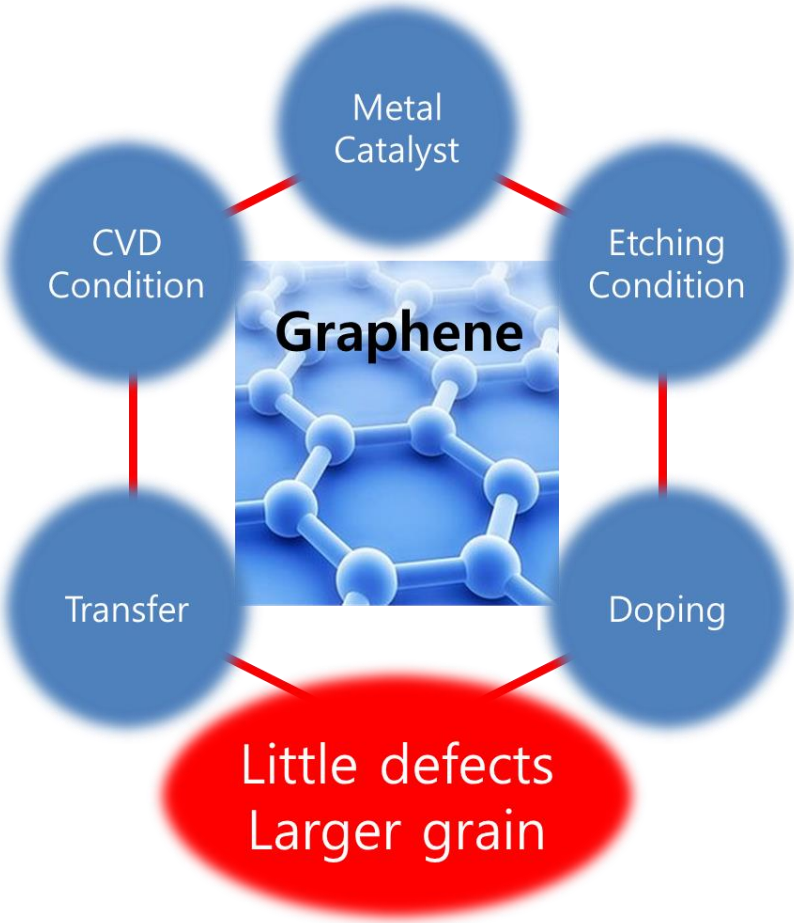

Figure 1.6. The important factors of CVD synthesis of high-quality graphene.

1.3. Defects of CVD graphene

1.3.1. Grain boundaries

H. Zhang et al.[9] reported that the electron scattering effect around the grain boundary can substantially reduce the carrier mobility of graphene. The heptagon and pentagon network at grain boundaries does disrupt the sp2 delocalization of π electrons in graphene. Decreasing the amount of domain boundary should be a key step for further enhancing the quality of CVD graphene. However, in the growth of CVD graphene, graphene islands nucleate from random locations. As the growth of such grains proceeds, they coalesce and eventually merge into an interconnected polycrystalline graphene. Furthermore, as their size increasing, single-crystal islands evolve into polycrystalline islands with increasing sizes, and especially in the graphene grown on Cu(100) than the graphene grown on Cu(111). [as shown in Table 1.2.][10]

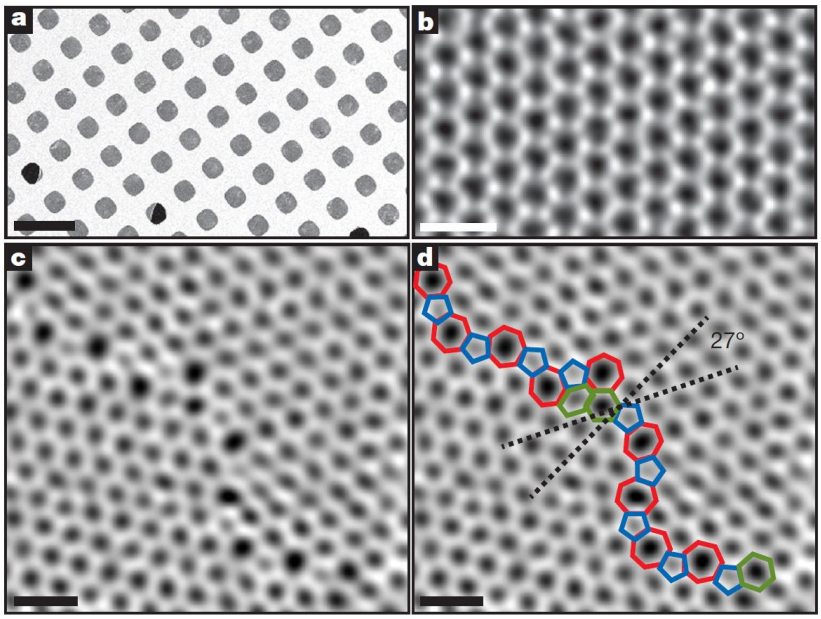

Figure 1.7. Atomic-resolution ADF-STEM images of graphene crystals. Two grains intersect with a 27° relative rotation. [Adapted from Ref. 11]

	<15 m (88 islands)	15-35 m (45 islands)	35-50 m (29 islands)
6-lobed islands	97.7%	66.7%	13.8%
4-lobed islands	96.6%	11.1%	3.4%

Table 1.2. Size dependent percentage of single-crystal 6- and 4-lobed graphene islands. [Adapted from Ref. 10]

1.3.2. Corrugated morphology

The interaction between the substrate and graphene strongly influences corrugated morphology formation. There are ripple, wrinkle, and folds in the corrugated morphology.(as shown in Figure 1.8.)

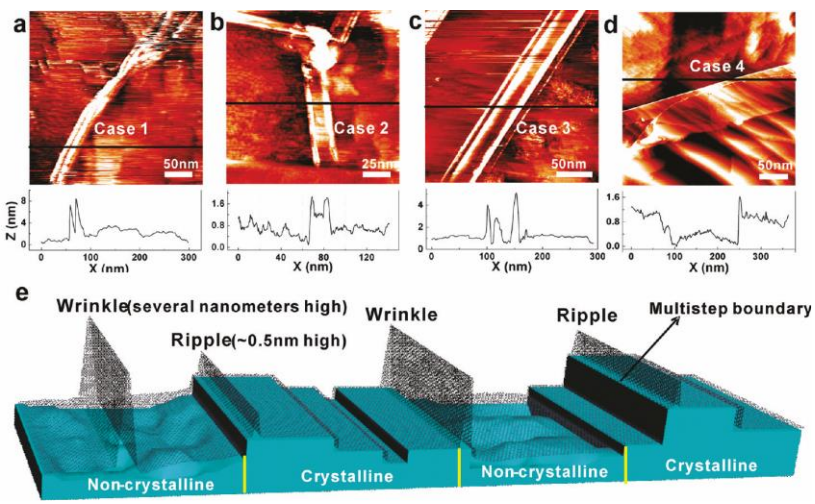

Figure 1.8. (a-d) STM morphology of crooked wrinkles on amorphous Cu subsrates and its height profile along the line direction. (e) Sketch map showing the positions of wrinkles and ripples with substrate states. [Adapted from Ref. 12]

During the cooling down process, which is inevitable process in thermal CVD growth. This leads to high density terraces and step edges Cu surface and graphene having high densities of corrugated morphology due to the different thermal expansion coefficients(TEC) of graphene and the metal catalyst.(as shown in Figure 1.9.)[13] This is because the TEC of graphene is negative ($-7\sim8 \times 10^{-6}K^{-1}$ at room temperature), but the typical metals has positive coefficients.

Figure 1.10. shows the corrugated Cu leads to quasi periodic nanoripple arrays of graphene after graphene transfer onto target substrates. The rippled graphene gives rise to flexural phonon scattering, which play a limiting role in charge mobility and sheet resistance.[14]

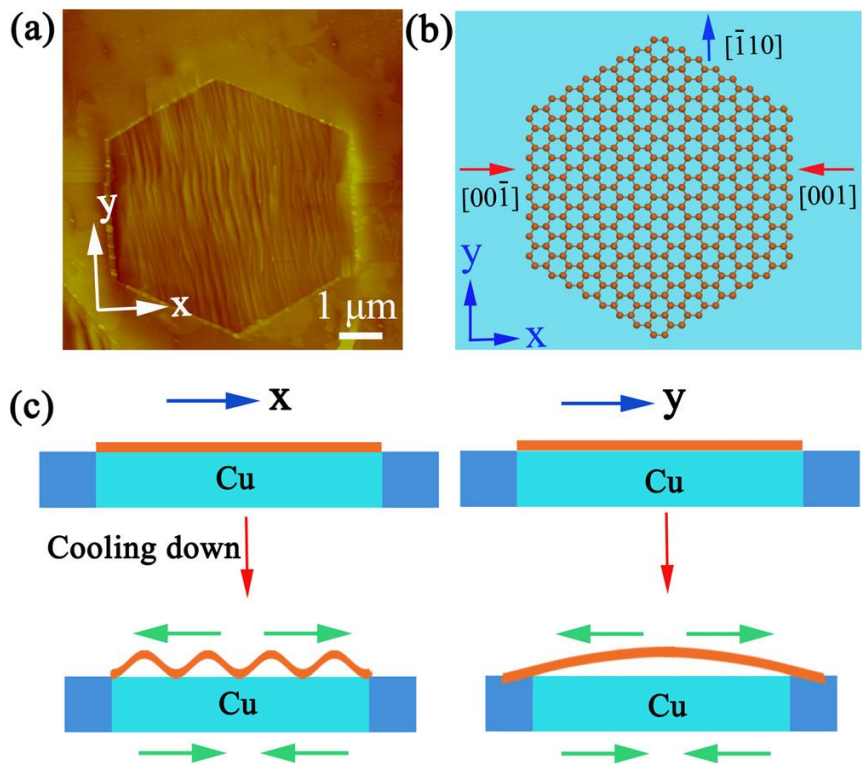

Figure 1.9. Wrinkles formation in CVD process (a) An AFM image of a hexagonal graphene island on Cu surface. (b) Schematic diagram showing the top view of a hexagonal graphene flake on Cu(110). (c) Schematic diagrams showing the effect of thermal expansion mismatch on the formation of graphene ripples. [Adapted from Ref. 13]

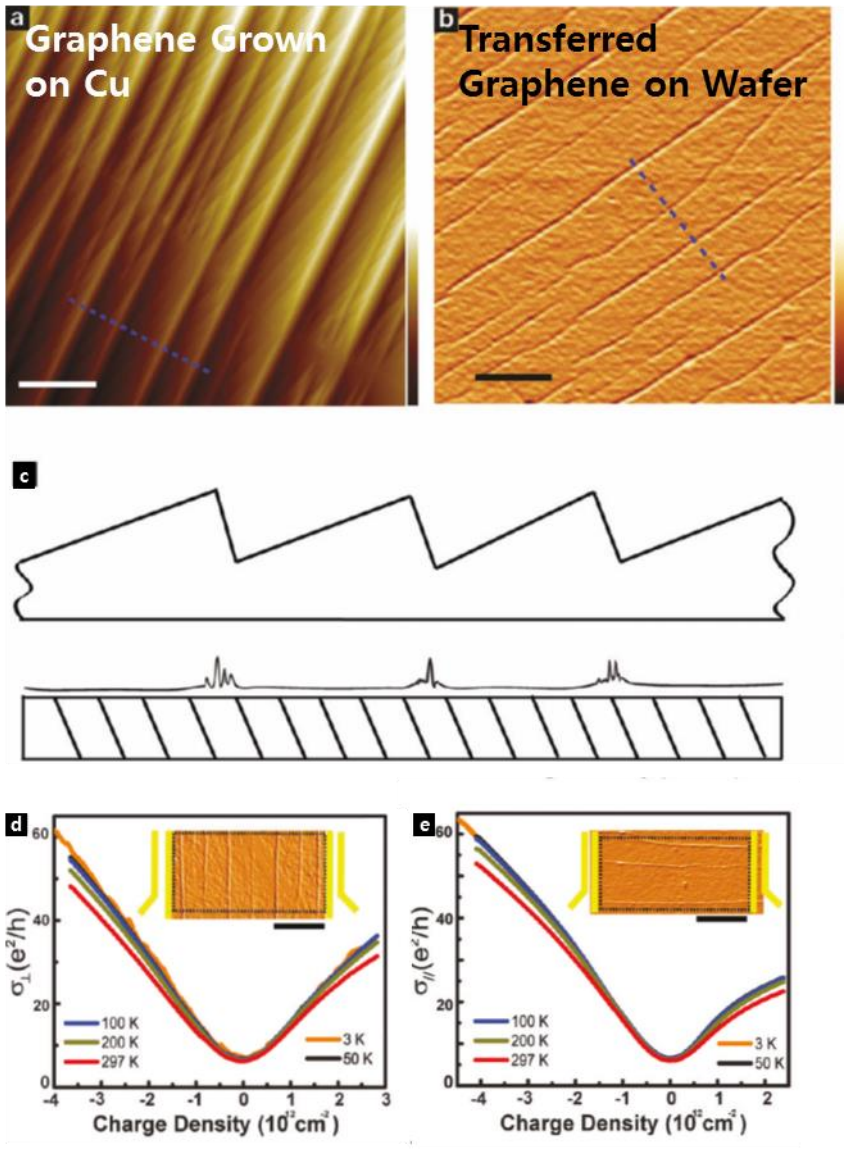

Figure 1.10. AFM images of (a) Cu surface and (b) CVD graphene on SiO_2. (c) AFM line scans reveal nanoripple arrays which are closely correlated with the Cu terraces. T-dependent sublinear conductivity for nanoripple arrays (d) parallel and (e) perpendicular configuration. [Adapted from Ref. 14]

1.4. Doping of graphene

Many scientists have studied to make high quality CVD graphene. However, due to high resistance, the pristine graphene still has problem to replace indium tin oxide (ITO). One of the solution is doping to tune the Fermi energy level of graphene.

The doping of graphene can be classified into two types, depending on the doping method, carrier injection and controlling the Fermi level. The carrier injection doping can be obtained by atom substitution or by making chemical bonding.(as shown in Figure 1.11.)[15] Although carrier injection doping has advantages in doping stability, it deforms the structure of graphene to lose inherent properties of graphene and resulting in high resistance.

Figure 1.12. shows doping can be obtained by controlling the Fermi level of graphene, which can be achieved by changing a gate voltage and by physisorption of chemical dopants on the graphene surface.[16] The conventional way to modify electrical properties of a graphene is the electric field effect by using the dielectric and applying gate voltage.(as shown in Figure 1.12. a and b) However, the gate voltage induced doping has a limitation in the size of doped graphene and its complexity in device fabrication process.

Fermi level of graphene can be easily tuned by physisorbed species on its surface, such as gases, chemicals, or metal particles.(as shown in Figure 1.13. c) The type of doping decided by electron withdrawing or donating group of dopants. Comparing to the carrier injection, the physisorption method can achieve low resistance due to its tunability, but it is insufficient in doping stability.

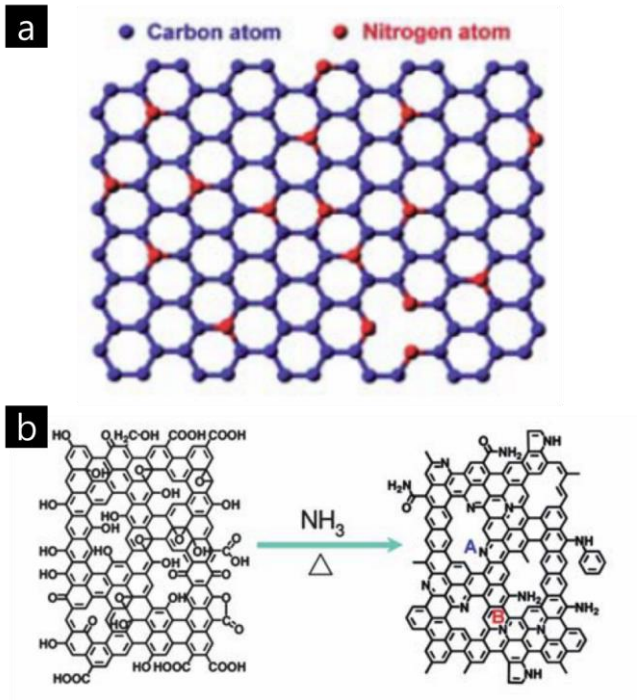

Figure 1.11. (a) A schematic representation of the nitrogen doped graphene. (b) A schematic of the structure of graphene oxide and its reaction with ammonia through thermal annealing. [Adapted from Ref. 15]

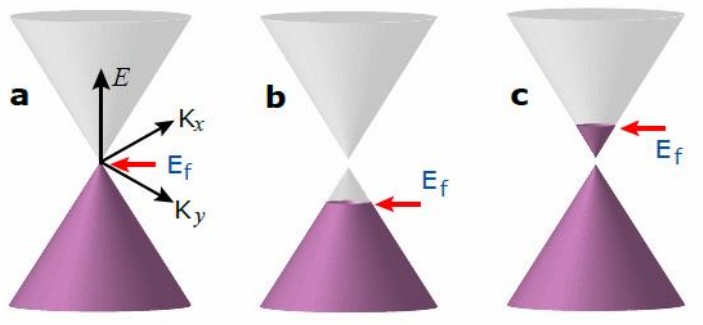

Figure 1.12. Schematic band structures of graphene. (a)Band structure of pristine graphene with zero bandgap. Band structures of (b) p-type and (c) n-type graphene with the bandgap. [Adapted from Ref. 16]

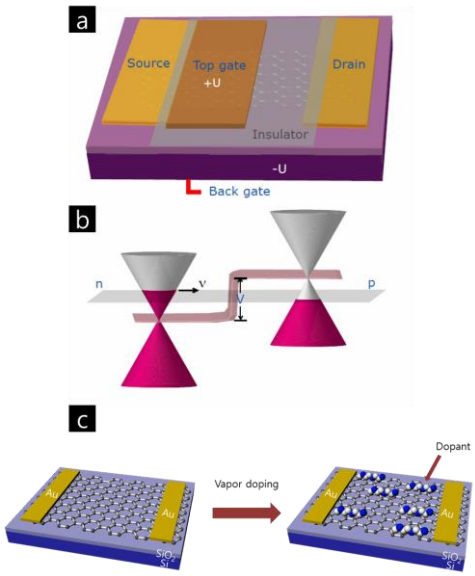

Figure 1.13. (a) The scheme of the graphene field effect transistor device. (b) The energy diagram shows a potential barrier with height V and the position of the Fermi level with respect to the touching point of the valence and the conduction bands. [Adapted from Ref. 16] (c) Schematic diagram of the vapor-phase doping process.

1.5. Scope of the Thesis

Graphene as the representative 2D materials has been widely studied due to its outstanding properties. In order to apply graphene films for various applications, we have synthesized the large-scale, high-quality graphene by CVD method. To obtain high-quality graphene films, we have conducted studies on three topics: (1) improvement of the catalytic properties of Cu for graphene synthesis, (2) diminishing corrugated morphology of graphene, and (3) development of stable and strong dopants for tuning of electric

properties.

This dissertation provides the details of my work on all projects related to synthesize and characterization of the graphene synthesis by CVD on copper and its application for field effect transistor. Especially, we will discuss the improvement of the sheet resistance of graphene by controlling synthesis condition. We also controlled the work function of graphene films via vapor phase doping process. These contents are reported in *Nanoscale*, *Physical Chemistry and Chemical Physics*.

1.6. References

1. A. K. Geim, and K. S. Novoselov, The rise of graphene. *Nature Materials* 2007, 6, 183.

2. K. S. Novoselov, and A. H. Castro Neto, Two-dimensional crystals-based heterostructures: materials with tailored properties. *Physica. Scripta* 2012, T146, 014006.

3. H. Terrones, R. Lv, M. , Terrones, and M. S. Dresselhaus, The role of defects and doping in 2D graphene sheets and 1D nanoribbons. *Rep. Prog. Phys.* 2012, 75, 062501.

4. C. Mattevi, H. Kim, and M. A Chhowalla, Review of chemical vapour deposition of graphene on copper. *J. Mater. Chem.* 2011, 21, 3324.

5. A. Reina, X. Jia, J. Ho, D. Nezich, H. Son, V. Bulovic, M. S. Dresselhaus, and J. Kong, Large area, few-layer graphene films on arbitrary substrates by chemical vapor deposition. *Nano Lett.* 2009, 9, 30.

6. N. A. Vinogradov, A. A. Zakharov, V. Kocevski, J. Rusz, K. A. Simonov, O. Eriksson, A. Mikkelsen, E. Lundgren, A. S. Vinogradov, N. Martensson, and A. B. Preobrajenski, Formation and structure of graphene waves on Fe(110). *Phys. Rev. Lett.* 2012, 109, 026101.

7. P. C. Rogge, S. Nie, K. F. McCarty, N. C. Bartelt, and O. D. Dubon, Orientation-dependent growth mechanisms of graphene islands on Ir(111). *Nano Lett.* 2015, 15, 170.

8. P. W. Sutter, J. I. Flege, and E. A. Sutter, Epitaxial graphene on ruthenium. *Nat. Mater.* 2008, 7, 406.

9. H. Zhang, G. Lee, C. Gong, L. Colombo, and K. Cho, Grain Boundary Effect on Electrical Transport Properties of Graphene. *The Journal of Physical Chemistry C* 2014, 118, 2338.

10. Y. Wu, Y. Hao, H. Y. Jeong, Z. Lee, S. Chen, W. Jiang, Q. Wu, R. D. Piner, J. Kang, and R. S. Ruoff, Crystal structure evolution of individual graphene islands during CVD growth on copper foil. *Adv. Mater*. 2013, 25, 6744.

11. P. Y. Huang, C. S. Ruiz-Vargas, A. M. van der Znde, W. S.Whitney, M. P. Levendorf, J. W. Kevek, S. Garg, J. S. Alden, C. J. Hustedt, Y. Zhu, J. Park, P. L. McEuen, and D. A. Muller, Grains and grain boundaries in single-layer graphene atomic patchwork quilts. *Nature* 2011, 469, 389.

12. Y. Zhang, T. Gao, Y. Gao, S. Xie, Q. Ji, K. Yan, H. Peng, and Z.Liu, Defect-like structures of graphene on copper foils for strain relief investigated by high-resolution scanning tunneling Microscopy. *ACS nano* 2011, 5, 4014.

13. L. Meng, Y. Su, D. Geng, G. Yu, Y. Liu, R. -F. Dou, J. -C. Nie, and L. He, Hierarchy of graphene wrinkles induced by thermal strain engineering. *Applied Physics Letters* 2013, 103, 251610.

14. G.-X. Ni, Y. Zheng, S. Bae, H. R. Kim, A. Pachoud, Y. S. Kim, C.-L. Tan, D. Im, J.-H. Ahn, B. H. Hong, and B. Ozyilmaz, Quasi-periodic nanoripples in graphene grown by CVD and its impact on charge transport. *ACS nano* 2012, 6, 1158.

15. H. Liu, Y. Liu, and D. Zhu, Chemical doping of graphene. *J. Mater. Chem.* 2011, 21, 3335.

16. B. Guo, L. Fang, B. Zhang, and J. R. Gong, Graphene Doping: A Review. *Insciences Journal*, 2011, 80.

Chapter 2. Tension-Controlled Single-Crystallization of Copper Foils for High-Quality Graphene Synthesis

2.1. Introduction

Graphene can be synthesized by chemical vapor deposition (CVD) on diverse metal catalysts such as Ir,[1] Ni,[2] Ru,[3] Fe,[4] and Cu.[5] Among them, Cu has been regarded as the most promising catalytic substrate owing to its lower cost and suitable carbon solubility that suppresses the growth of multilayers.[6]

However, the electrical properties of the CVD-grown graphene are not as good as those of exfoliated graphene because of its polycrystallinity and grain boundary originated from the randomly oriented nucleation and growth of graphene islands.[7,8] It was reported that the Cu (111) surface showing only 3~4% lattice mismatch with graphene decreases the defect density of graphene, and thus, enhances the electrical property.[9] The Cu (111) substrates were typically obtained by the deposition and annealing of thin Cu films on sapphire or SiO_2 wafers with limited size and cost.[10-12](Figure 2.1.a and c) The annealing of polycrystalline Cu foils can induce the recrystallization into Cu (111), but it usually takes more than 12 hours.[13](Figure 2.1.c)

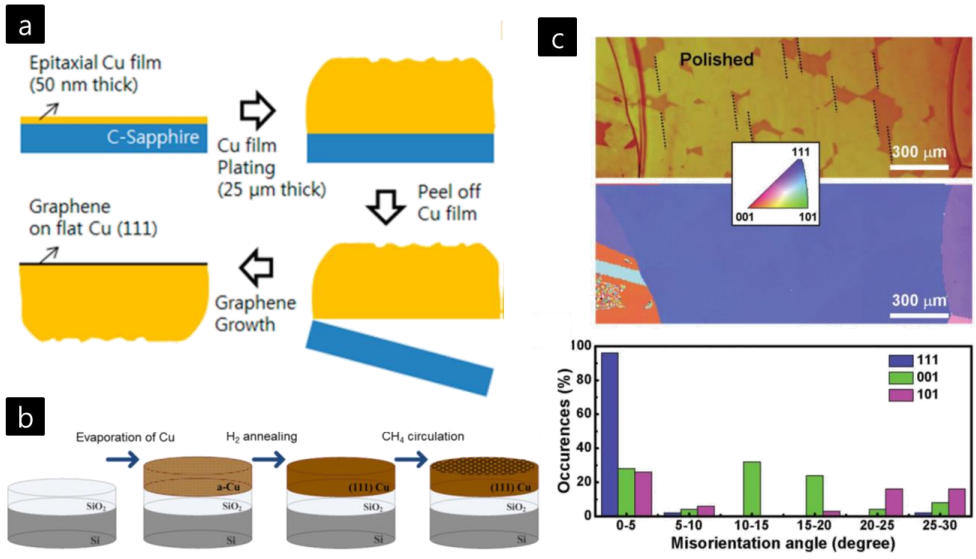

Figure 2.1. The methods to obtain Cu(111) substrates. Cu deposition on (a) sapphire and (b) SiO_2 wafer. Cu(111) was obtained by prolonged annealing. [Adapted from Ref. 10, 12, and 13]

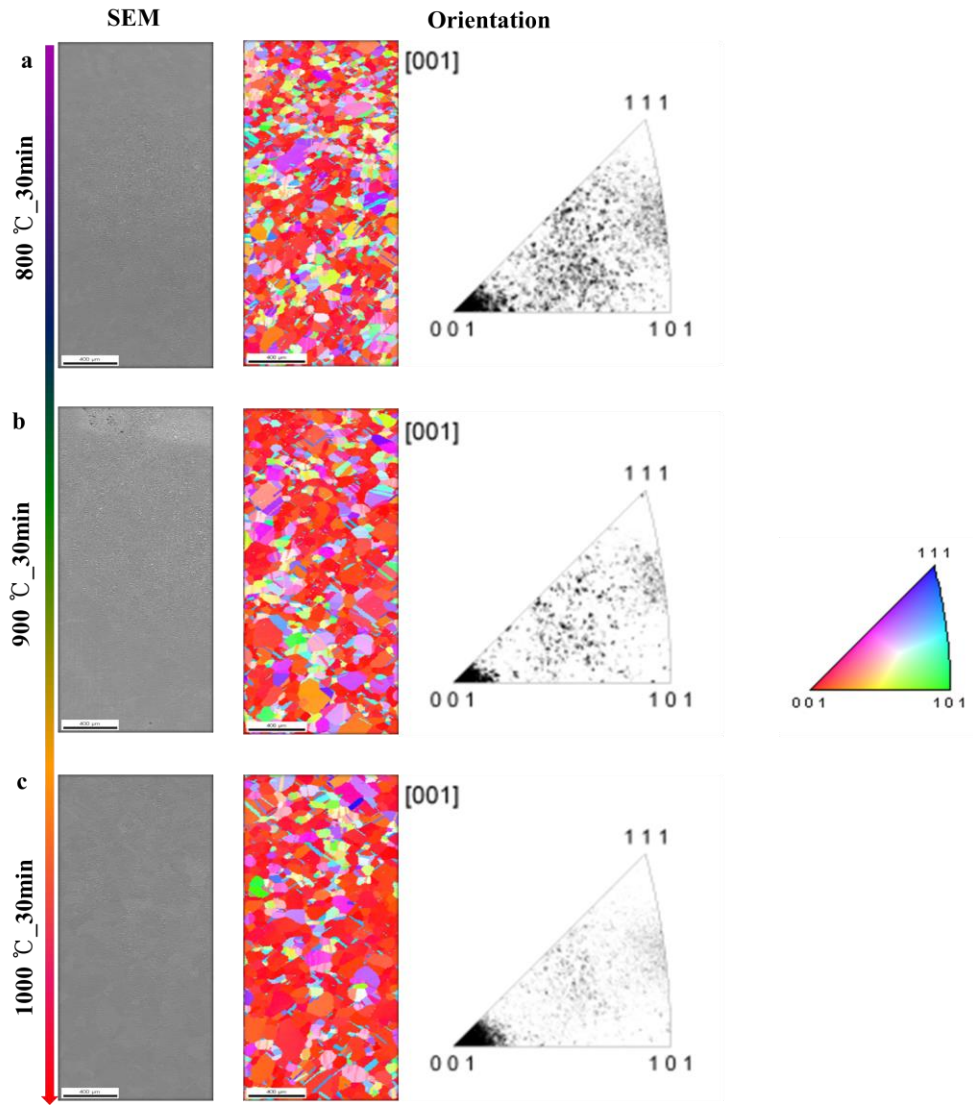

Figure 2.2. Surface orientation of CVD processed Cu foil at different temperatures. (a) 800, (b) 900, and (c) 1000 °C.

On the other hand, as shown in Figure 2.2., conventional thin copper foils are known to show Cu (100) orientation dominantly after the CVD synthesis that is typically 1~2 hours long.[14, 15] The grain boundary energy is closely related to abnormal grain growth (AGG) in various metals,[16-20] which can be controlled by

mechanical tension. This tension-controlled recrystallization condition can be created by vertically suspending Cu foils with variable tension during the CVD synthesis of graphene. The vertical tension at ~970 °C promotes the dynamic recrystallization into small grains first and then induces secondary recrystallization into larger grains other than Cu (100), which is common orientation for cold roll-pressed Cu foils.[16] Thus, we tried to optimize the vertical tension on the suspended Cu foils to find the recrystallization condition for Cu (111), and characterized the results after annealing only and after graphene synthesis by Raman spectroscopy, transmission electron microscopy (TEM), electron back-scattered diffraction (EBSD), X-ray diffraction (XRD), electron transport measurements, *etc*.

2.2. Experimental

2.2.1. Graphene synthesis

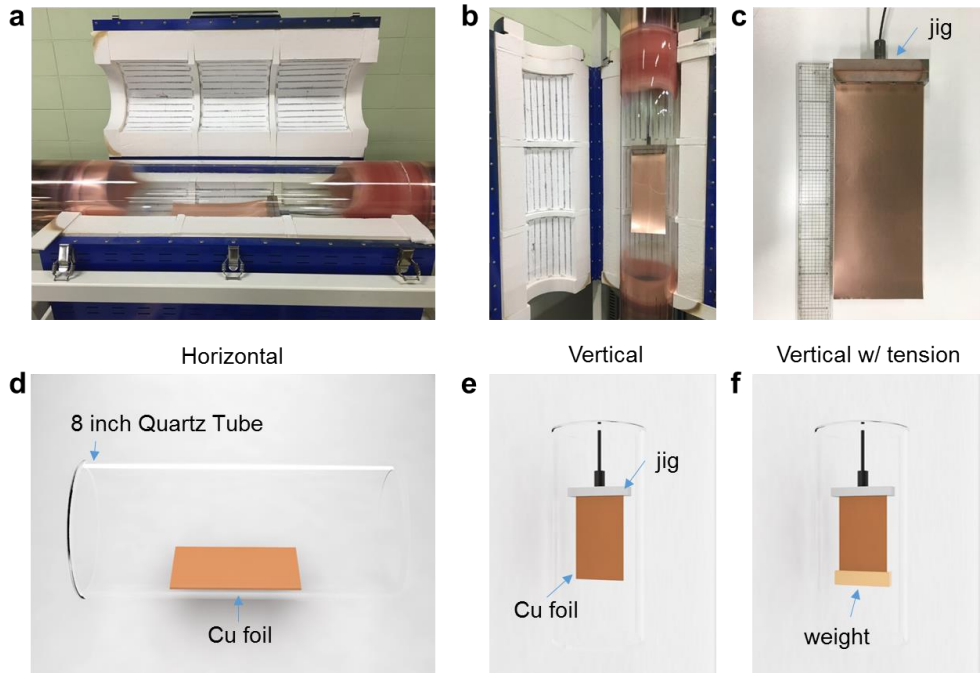

Figure 2.3. (a-c) Photographs of a horizontal-vertical switchable CVD system and a holding jig. (d, e) Schematic illustrations of horizontally and vertically loaded Cu foils without additional tension, respectively. (f) A schematic illustration of a vertically loaded Cu foil with tension applied by a weight. (g) An illustration of the in situ switchable horizontal-vertical CVD system, which provides identical growth conditions except the vertical tension by gravitation or additional weights applied to Cu foils.

Figure 2.3. shows the photographs and illustrations of a horizontal-vertical switchable CVD setup with an 8-inch quartz tube,

which provides an identical growth conditions except the vertical tension by gravitation or additional weights applied to Cu foils. Graphene was synthesized using a 13 cm wide, 30 cm long, and 25 μm thick polycrystalline Cu foil (99.7%) as a catalytic substrate with flowing 50 sccm H_2 for 1 hour at 970 °C under a pressure of 3.8 x 10^{-1} Torr. Next, methane was introduced into the chamber at a flow rate of 50 sccm with maintaining the chamber pressure at 8.8 x 10^{-1} Torr during the growth for 30 min. Finally, the furnace was slowly cooled down to room temperature with flowing H_2 only. For the vertical synthesis, the upper edge of the Cu foil was fixed at the holding jig (Figure 2.3.c) and suspended as shown in Figure 2.3c and 2.3.e. The vertical tension was applied by attaching additional weight along the other edge (Figure 2.3.f), which were compared with the results from the horizontal growth setup (Figure 2.3.d).

2.2.2. TEM mapping

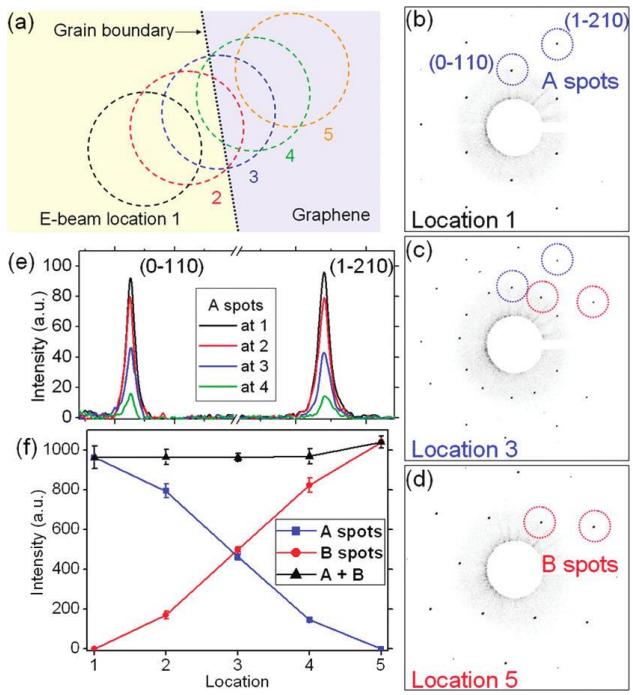

Figure 2.4. Grain boundary(GB) identification through diffraction series on a graphene sheet. (adapted from reference [22])

We carried out the grain boundary analyses of graphene by scanning diffraction mapping in TEM after transferring the graphene prepared by a direct transfer method on TEM grid.[21] As shown in Figure 2.4., multiple selected area electron diffractions(SAEDs) are collected as we scan the beam spots, and the positions that show the rotation of the SAEDs are marked with dots on bright-field TEM images. By repeating this process, it is possible to map the grain boundaries of graphene at much larger scale than the case of using a dark-field TEM method.[7, 22]

2.3.3. FET fabrication and its mobility calculation

The electrical properties of graphene was characterized by fabricating and measuring back gated field-effect-transistors (FETs), where the charge carrier mobility can be determined by calculated by the following equation in the linear regime: [23]

$$I_D = \frac{WC_i}{L} V_D \mu (V_G - V_T) \qquad (1)$$

where C_i = 1.08 × 10^{-8} F cm^{-2}, V_D = 0.01 V, W = 230 μm, and L = 180 μm.

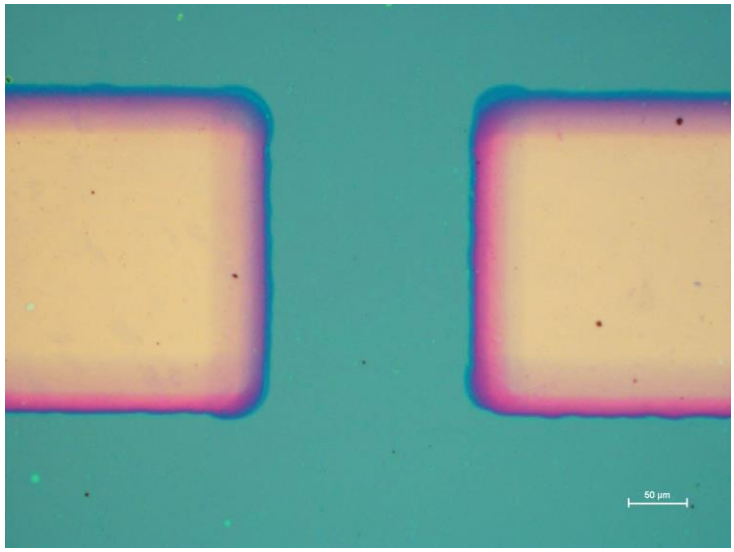

Figure 2.5. Optical microscope image of graphene field effect transistor, scale bar = 50 m.

2.4. Results and Discussion

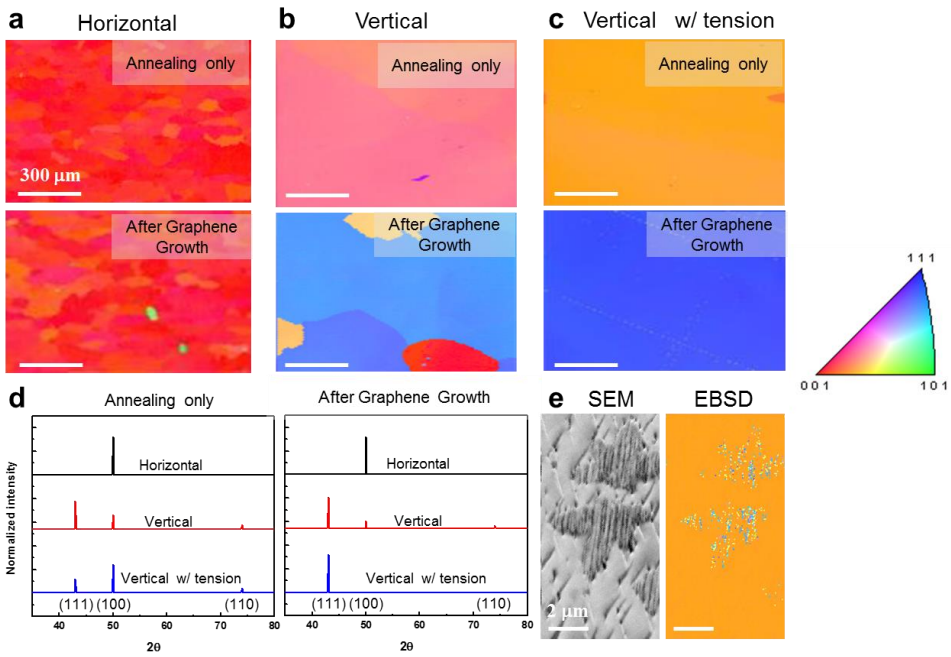

Figure 2.6. (a-c) EBSD images of annealed and graphene-grown Cu surface with horizontal/vertical geometry with/without tension control. (d) XRD spectra of annealed and graphene-grown Cu surface with and without tension control. The 2Θ measured from 30° to 80° shows the three intense peaks at 43°, 50°, and 74°, which are assigned to Bragg reflections from the surface of Cu (111), (100), and (110), respectively. (e) SEM and EBSD images of graphene islands of Cu, indicating that the recrystallization of Cu surface can be promoted by graphene in the case of tension-controlled growth.

Figures 2.6.a-b show the EBSD analyses of the annealed Cu foils at 970 °C and the graphene-grown Cu foils that are horizontally and vertically loaded in a growth chamber, indicating that the crystallinity

of Cu is relatively uncontrollable and small. It is well known that a cold roll-pressed Cu foil usually shows (100) orientation, following the strain energy release maximization model.[14, 15] On the other hand, Figure 2.6.c shows the case of the vertically loaded Cu foils with tension induced by adding a weight twice heavier than the Cu foil, exhibiting that the crystalline orientation of Cu can be controlled in large scale. The average grain sizes of the graphene-grown Cu are increased from 87.1 μm. to ~ 2,000 μm after applying the tension, which is expected to correlate with the crystalline sizes of graphene. Figure 2.6.d shows the XRD patterns of the Cu corresponding to Figures 2.6.a-c, indicating that the vertically loaded Cu with tension before graphene growth shows the mixture of (111) and (100) orientations, while the horizontally loaded Cu foils still exhibit (100) dominant orientation. This implies that higher mobility of (111) tilt grain boundaries than those of (100) tends to promote the partial abnormal grain growth (AGG) into (111) during the annealing process.[24, 25] This AGG can be promoted by applying mechanical tensions on Cu. which has been used to large scale growth of single-crystalline metals,[26] but the annealed-only Cu foils don't show perfect a single crystalline surface with low index facets even with the tension applied by 30 times weight of Cu.

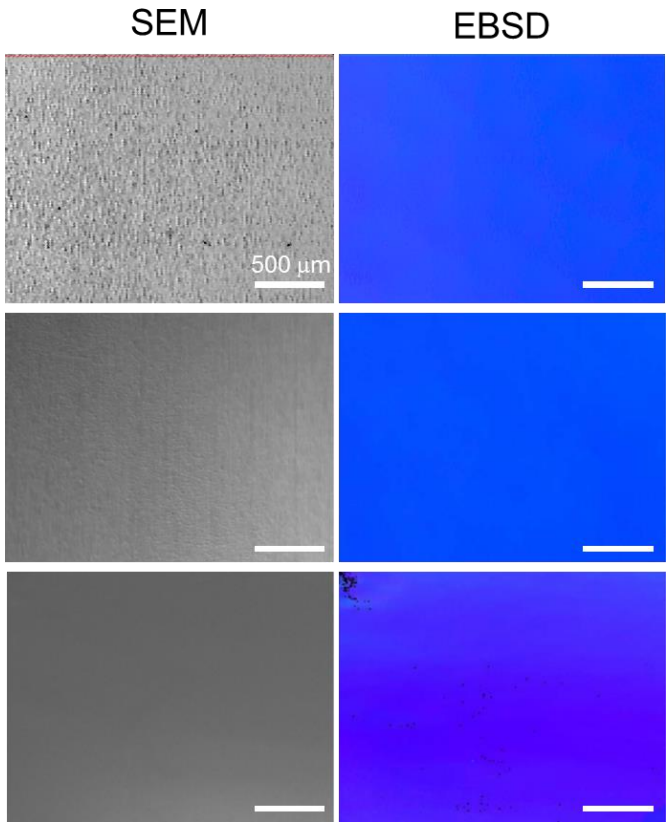

Figure 2.7. SEM and EBSD images obtained from 3 different batches at the same position on the graphene-grown Cu foils that are vertically loaded with controlled tension, indicating that the single-crystallization into Cu is reproducible.

However, it is surprising that the growth of graphene dramatically catalyzes the recrystallization into (111) dominant surfaces as shown in the lower part of Figure 2.6.c. The EBSD image of the graphene island after 1 min growth on the vertically loaded Cu with controlled tension clearly shows that the crystalline orientation of the graphene-covered region begins to change (Figure 2.6.e and Figure 2.7.), while the bare Cu surface still maintains the (100) orientation.

We suppose that the hexagonal lattice of graphene with a better match with Cu (111) surface than (100) results in less surface energy at the interface, promoting the crystallization into (111) cooperatively with the applied tension. Thus, the graphene-grown Cu surface with vertical tension exhibit almost (111) single-crystalline orientation at large scale as evidenced by the EBSD and XRD results in Figure 2.6. c-d and Figure 2.8.

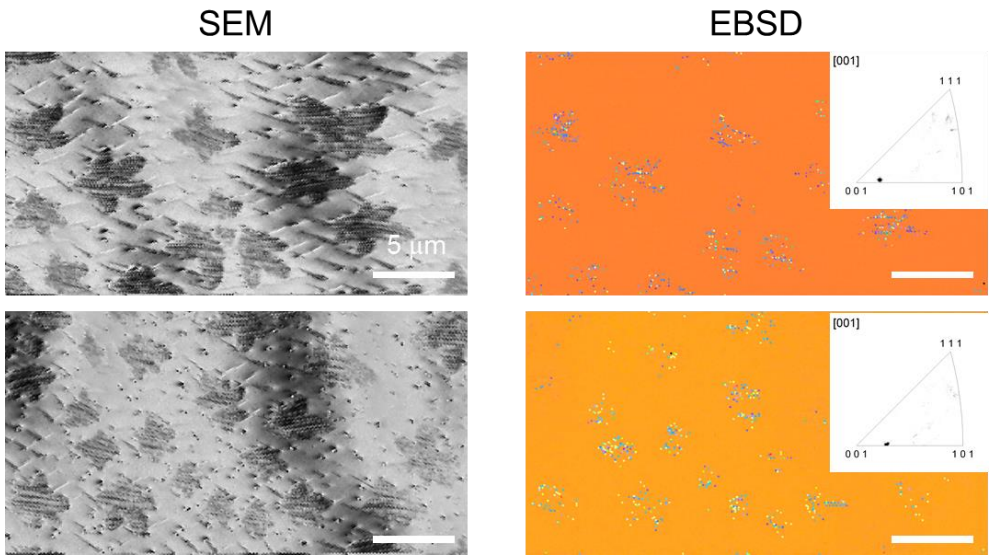

Figure 2.8. SEM and EBSD images of partially grown graphene islands on a vertically loaded Cu foil with controlled tension. The Cu surface underneath graphene islands tends to be reoriented by the interaction with graphene lattice at the interface.

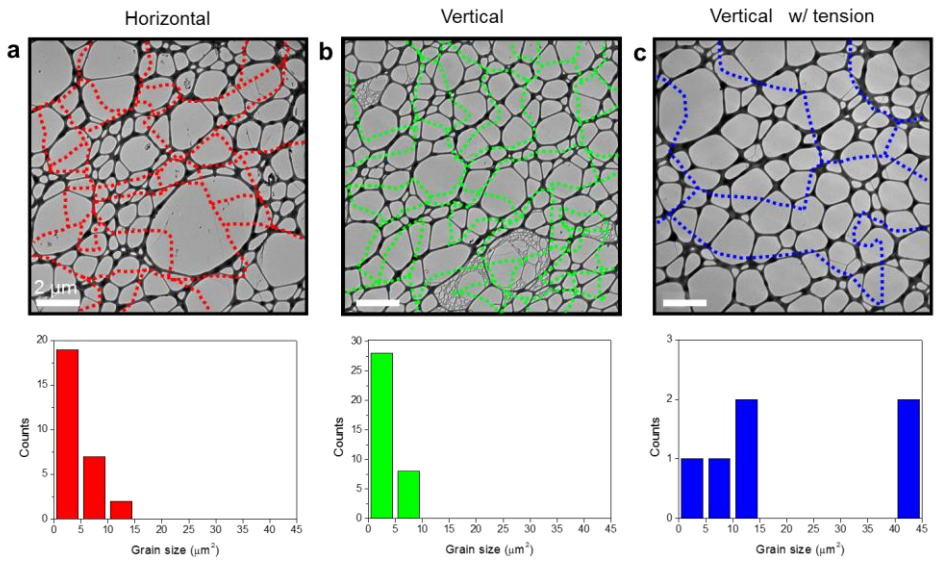

Figure 2.9. Grain boundary analyses of graphene by scanning diffraction mapping in TEM, indicating that the graphene from vertically loaded Cu with tension (c) shows the larger domain sizes than the cases of the horizontally loaded Cu (a) and the vertically loaded Cu without additional tension (b).

It has been reported the crystallographic orientations of the catalytic substrates affect the quality as well as the growth rate of graphene film,[27, 28] which is also possibly related to larger domain sizes of the graphene as the growth on Cu (111) minimizes misalignment between growing graphene islands. The histograms in Figure 2.9. a-c indicate that the mean grain sizes are 4.24 ± 3.21, 3.41 ± 2.60, and 22.41 ± 15.62 μm^2 for the horizontal, vertical, and vertical Cu with tension, respectively. The result implies that there is strong correlation between the grain size of graphene and the crystalline orientation of the underlying Cu substrates, and the dynamic grain evolution can be less hindered when the growing

graphene is interfaced with Cu (111) surface.[29, 30]

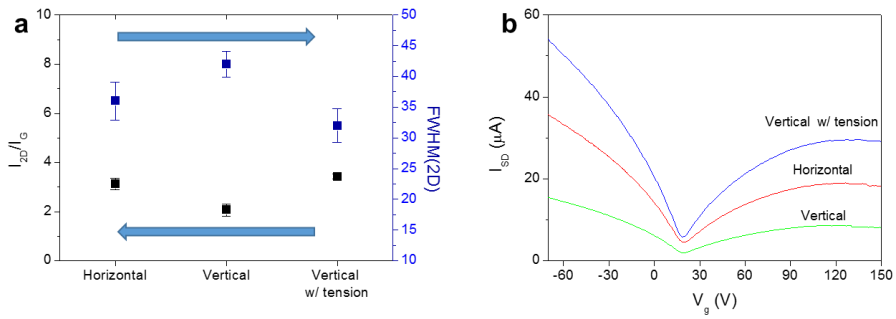

Figure 2.10. (a) FWHM(2D) and I(2D)/I(G) values for the Raman spectra (excitation λ = 514 nm) of the horizontal, vertical, and vertical Cu with tension, corresponding to Fig. 1d-e, respectively.). Raman spectroscopy was performed using a 514 nm laser (b) Field-effect transistor (FET) characteristics of graphene grown on the horizontal (red), vertical (green), and vertical Cu with tension (blue), showing the highest conductance and carrier mobility of the graphene grown on Cu (111).

The Raman analyses in Figure 2.10.a show that the 2D FWHM values are 36.8 ± 3.1, 42.4 ± 2.1, and 32.1 ± 2.7 cm^{-1}, and the I(2D)/I(G) ratios are 3.1 ± 0.2, 2.01 ± 0.3, and 3.4 ± 0.1 for the graphene synthesized from the horizontal, vertical, and vertical Cu with tension, respectively. This indicates that the graphene grown on the vertically loaded Cu with tension shows the highest quality and lower doping due to the lower density of graphene boundaries.[31]

Figure 2.10.b shows mobilities extracted from four-point transport measurements. The room temperature FET mobilities are 4376 ±

334, 2044 ± 531, and 6913 ± 207 $cm^2V^{-1}s^{-1}$ for the graphene synthesized from the horizontal, vertical, and vertical Cu with tension, respectively. Thus, we conclude that the (111) dominant Cu surface promotes the larger grain growth of graphene, leading to the enhanced electrical properties of graphene.

2.5. Conclusions

In conclusion, we demonstrate a new method to optimize the crystalline orientations of vertically suspended Cu foils by tension control, resulting in large-area recrystallization into Cu (111) surface as the applied tension activates the grain boundary energy of Cu and promotes its abnormal grain growth to single crystals as evidenced by SEM, EBSD and XRD analyses. In addition, we found a clue that the formation of graphene cooperatively assists the recrystallization into Cu (111) by minimizing the surface energy of Cu at the interface with graphene.[32] The domain sizes and electrical properties of graphene grown on the single crystalline Cu (111) are compared with those of graphene from Cu (100), The mean graphene grain size of graphene grown on tension-controlled Cu foil (22.41 μm^2) is ~5 times larger than that from the horizontal furnace (4.24 μm^2), and the charge carrier mobility is measured to be enhanced by ~50%. This implies that the less lattice mismatch and the lower interaction energy between Cu (111) and graphene allows the growth of larger single-crystalline graphene with higher electrical quality. We believe that our finding provides a crucial idea to design a system for the CVD growth of high-quality graphene films on roll-to-roll (R2R) Cu foils, where the tension control is inevitably involved, which would be of great importance for the continuous mass-production of graphene films for practical applications in the future.[33-39]

2.6. References

1. P. C. Rogge, K. Thurmer, M. E. Foster, K. F. McCarty, O. D. Dubon and N. C. Bartelt, Real-Time Observation of Epitaxial Graphene Domain Reorientation. *Nat. Commun.* 2015, 6, 6880.

2. K. S. Kim, Y. Zhao, H. Jang, S. Y. Lee, J. M. Kim, K. S. Kim, J. H. Ahn, P. Kim, J. Y. Choi and B. H. Hong, Large-Scale Pattern Growth of Graphene Films for Stretchable Transparent Electrodes. *Nature* 2009, 457, 706.

3. P. W. Sutter, J. I. Flege and E. A. Sutter, Epitaxial Graphene on Ruthenium. *Nat. Mater.* 2008, 7, 406.

4. N. A. Vinogradov, A. A. Zakharov, V. Kocevski, J. Rusz, K. A. Simonov, O. Eriksson, A. Mikkelsen, E. Lundgren, A. S. Vinogradov, N. Martensson and A. B. Preobrajenski, Formation and structure of graphene waves on Fe(110). *Phys. Rev. Lett.* 2012, 109, 026101.

5. S. Bae, H. Kim, Y. Lee, X. Xu, J. S. Park, Y. Zheng, J. Balakrishnan, T. Lei, H. R. Kim, Y. I. Song, Y. J. Kim, K. S. Kim, B. Ozyilmaz, J. H. Ahn, B. H. Hong and S. Iijima, Roll-to-Roll Production of 30-in. Graphene Films for Transparent Electrodes. *Nat. Nanotechnol.* 2010, 5, 574.

6. C. Mattevi, H. Kim and M. Chhowalla, A Review of Chemical Vapour Deposition of Graphene on Copper. *J. Mater. Chem.* 2011, 21, 3324.

7. P. Y. Huang, C. S. Ruiz-Vargas, A. M. van der Zande, W. S. Whitney, M. P. Levendorf, J. W. Kevek, S. Garg, J. S. Alden, C. J.

Hustedt, Y. Zhu, J. Park, P. L. McEuen and D. A. Muller, Grains and Grain Boundaries in Single-Layer Graphene Atomic Patchwork Quilts. *Nature* 2011, 469, 389.

8. Q. Yu, L. A. Jauregui, W. Wu, R. Colby, J. Tian, Z. Su, H. Cao, Z. Liu, D. Pandey, D. Wei, T. F. Chung, P. Peng, N. P. Guisinger, E. A. Stach, J. Bao, S. S. Pei and Y. P. Chen, Control and Characterization of Individual Grains and Grain Boundaries in Graphene Grown by Chemical Vapour Deposition. *Nat. Mater.* 2011, 10, 443.

9. H.-J. Shin, S.-M. Yoon, W. M. Choi, S. Park, D. Lee, I. Y. Song, Y. S. Woo and J.-Y. Choi, Influence of Cu Crystallographic Orientation on Electron Transport in Graphene. *Appl. Phys. Lett.* 2013, 102, 163102.

10. B. Hu, H. Ago, Y. Ito, K. Kawahara, M. Tsuji, E. Magome, K. Sumitani, N. Mizuta, K.-i. Ikeda and S. Mizuno, Epitaxial Growth of Large-Area Single-Layer Graphene Over Cu(111)/Sapphire by Atmospheric Pressure CVD. *Carbon* 2012, 50, 57.

11. H. K. Yu, K. Balasubramanian, K. Kim, J.-L. Lee, M. Maiti, C. Ropers, J. Krieg, K. Kern and A. M. Wodtke, Chemical Vapor Deposition of Graphene on a "Peeled-Off" Epitaxial Cu(111) Foil: A Simple Approach to Improved Properties. *ACS nano* 2014, 8, 8636.

12. L. Tao, J. Lee, M. Holt, H. Chou, S. J. McDonnell, D. A. Ferrer, M. G. Babenco, R. M. Wallace, S. K. Banerjee, R. S. Ruoff and D. Akinwande, Uniform Wafer-Scale Chemical Vapor Deposition of Graphene on Evaporated Cu (111) Film with Quality Comparable to

Exfoliated Monolayer. *J. Phys. Chem. C* 2012, 116, 24068.

13. L. Brown, E. B. Lochocki, J. Avila, C. J. Kim, Y. Ogawa, R. W. Havener, D. K. Kim, E. J. Monkman, D. E. Shai, H. I. Wei, M. P. Levendorf, M. Asensio, K. M. Shen and J. Park, Polycrystalline Graphene with Single Crystalline Electronic Structure. *Nano Lett.* 2014, 14, 5706.

14. P. Gerber, J. Tarasiuk, T. Chauveau, B. and A. Bacroix, Quantitative Analysis of the Evolution of Texture and Stored Energy during Annealing of Cold Rolled Copper. *Acta Mater.* 2003, 51, 6359.

15. S.-H. Hong and D. N. Lee, The Evolution of The Cube Recrystallization Texture in Cold Rolled Copper Sheets. *Mater. Sci. Eng. A* 2003, 351, 133.

16. N. Mortazavi, N. Bonora, A. Ruggiero and M. Hörnqvist Colliander, Dynamic Recrystallization During High-Strain-Rate Tension of Copper. *Metall. Mater. Trans. A* 2016, 47, 2555.

17. H. Chun, S.-M. Na, C. Mudivarthi and A. B. Flatau, The Role of Misorientation and Coincident Site Lattice Boundaries in Goss-Textured Galfenol Rolled Sheet. *J. Appl. Phys.* 2010, 107, 09A960.

18. H. Chun, S.-M. Na, J.-H. Yoo, M. Wuttig and A. B. Flatau, Tension and Strain Annealing for Abnormal Grain Growth in Magnetostrictive Galfenol Rolled Sheet. *J. Appl. Phys.* 2011, 109, 07A941.

19. D. L. Worthington, N. A. Pedrazas, P. J. Noell and E. M. Taleff,

Dynamic Abnormal Grain Growth in Molybdenum. *Metall. Mater. Trans. A* **2013**, 44, 5025.

20. J.-K. Chang, K. Takata, K. Ichitani and E. M. Taleff, Abnormal Grain Growth and Recrystallization in Al-Mg Alloy AA5182 Following Hot Deformation. *Metall. Mater. Trans. A* **2010**, 41, 1942.

21. W. Regan, N. Alem, B. Alemán, B. Geng, C. Girit, L. Maserati, F. Wang, M. Crommie and A. Zettl, A Direct Transfer of Layer-Area Graphene. *Appl. Phys. Lett.* **2010**, 96, 113102.

22. K. Kim, Z. Lee, W. Regan, C. Kisielowski, M. F. Crommie and A. Zettl, Grain Boundary Mapping in Polycrystalline Graphene. *ACS nano* **2011**, 5, 2142.

23. I. Jo, Y. Kim, J. Moon, S. Park, J. S. Moon, W. B. Park, J. S. Lee and B. H. Hong, Stable n-Type Doping of Graphene via High-Molecular-Weight Ethylene Amines. *Phys. Chem. Chem. Phys.* **2015**, 17, 29492.

24. H. Park and D. N. Lee, The Evolution of Annealing Textures in 90 Pct Drawn Copper Wire. *Metall. Mater. Trans. A* **2003**, 34, 531.

25. S. B. Lee, D.-I. Kim, S.-H. Hong and D. N. Lee, Texture Evolution of Abnormal Grains with Post-Deposition Annealing Temperature in Nanocrystalline Cu Thin Films. *Metall. Mater. Trans. A* **2012**, 44, 152.

26. E. M. Taleff and N. A. Pedrazas, A New Route for Growing Large Grains in Metals. *Science* **2013**, 341, 1461.

27. J. D. Wood, S. W. Schmucker, A. S. Lyons, E. Pop and J. W. Lyding, Effects of Polycrystalline Cu Substrate on Graphene Growth by Chemical Vapor Deposition. *Nano Lett.* 2011, 11, 4547.

28. P. C. Rogge, S. Nie, K. F. McCarty, N. C. Bartelt and O. D. Dubon, Orientation-Dependent Growth Mechanisms of Graphene Islands on Ir(111). *Nano Lett.* 2015, 15, 170.

29. S. Vollmer, G. Witte and C. Wöll, Determination of Site Specific Adsorption Energies of CO on Copper. *Catal. Lett.* 2001, 77, 97.

30. Y. Wu, Y. Hao, H. Y. Jeong, Z. Lee, S. Chen, W. Jiang, Q. Wu, R. D. Piner, J. Kang and R. S. Ruoff, Crystal Structure Evolution of Individual Graphene Islands During CVD Growth on Copper Foil. *Adv. Mater.* 2013, 25, 6744.

31. L. G. Cançado, A. Jorio and M. A. Pimenta, Measuring the Absolute Raman Cross Section of Nanographites as a Function of Laser Energy and Crystallite Size. *Phys. Rev. B* 2007, 76, 6.

32. J. H. Kang, J. Moon, D. J. Kim, Y. Kim, I. Jo, C. Jeon, J. Lee and B. H. Hong, Strain Relaxation of Graphene Layers by Cu Surface Roughening. *Nano Lett.* 2016, 16, 5993.

33. Y.-J. Kim, Y. Kim, K. Novoselov and B. H. Hong, Engineering Electrical Properties of Graphene: Chemical Approaches. *2D Mater.* 2015, 2, 042001.

34. J. Kang, D. Kim, Y. Kim, J.-B. Choi, B. H. Hong and S. W. Kim, High-Performance Near-Field Electromagnetic Wave Attenuation in Ultra-Thin and Transparent Graphene Films. *2D Mater.* 2017, 4, 025003.

35. S. Kang, H. Choi, S. B. Lee, S. C. Park, J. B. Park, S. Lee, Y. Kim and B. H. Hong, Efficient Heat Generation in Large-Area Graphene Films by Electromagnetic Wave Absorption. *2D Mater.* 2017, 4, 025037.

36. Y. Lee, S. Bae, H. Jang, S. Jang, S.-E. Zhu, S.-H. Sim, Y.-I. Song, B. H. Hong and J. H. Ahn, Wafer-Scale Synthesis and Transfer of Graphene Films. *Nano Lett.* 2010, 10, 490.

37. J. Kang, H. Kim, K. S. Kim, S. K. Lee, S. Bae, J. H. Ahn, Y. J. Kim, J. B. Choi and B. H. Hong, High-Performance Graphene-Based Transparent Flexible Heaters. *Nano Lett.* 2011, 11, 5154.

38. T.-H. Han, Y. Lee, M.-R. Choi, S.-H. Woo, S.-H. Bae, B. H. Hong, J.-H. Ahn and T.-W. Lee, Extremely Efficient Flexible Organic Light-Emitting Diodes with Modified Graphene Anode. *Nat. Photonics* 2012, 6, 105.

39. S. Bae, S. J. Kim, D. Shin, J. H. Ahn and B. H. Hong, Towards Industrial Applications of Graphene Electrodes. *Phys. Scripta* 2012, 014024.

Chapter 3. Controlling the Ripple Density and Heights: a New Way to Improve the Electrical Performance of CVD-Grown Graphene

Parts of this chapter have been published in:

W.-H. Park,[†] I. Jo,[†] B. H. Hong[*] and H. Cheong[*], *Nanoscale* 2016, **8**, 9822.

3.1. Introduction

Graphene, a 2-dimensional building block of a honey-comb structured carbon lattice, has been intensively studied for the past several years owing to its exceptional mechanical and electronic properties including an unusually high mobility of the charge carriers.[1] Significant progress for understanding various properties of graphene has stemmed from studying graphene flakes mechanically exfoliated from bulk graphite.[1, 2] Although these small flakes (<100 × 100 μm^2) are suitable for exploring the fundamental properties of intrinsic graphene, they are not appropriate for the evaluation of large area graphene-based products. Recently, chemical vapor deposition (CVD) technology using CH_4 and H_2 onto Cu foils to form large area graphene sheets is regarded as a promising way for mass production of large size transparent conducting graphene films for flexible electronics.[3,4]

However, many challenging issues in CVD-grown graphene products still remain such as irregularly distributed defects of various kinds[5] and volatile dopants that are easily removed during the reliability test, leading to changes in the sheet resistance value (R_s). Some alternatives such as hybridizing a graphene sheet with metallic nanowires have been developed. Integration of two-dimensional graphene and one-dimensional Ag nanowires in a hybrid film can significantly enhance electrical properties such as lower R_s and robustness against electrical breakdown, with negligible degradation of the optical transmittance.[6] In order to increase the quality of CVD-grown graphene, Park and co-workers[7] reported that variation of the cooling rate and the hydrocarbon concentration in the cooling step has yielded graphene islands with different sizes, nuclear densities, and growth rates. Hence, the nucleation site density on a Cu substrate was greatly reduced when a fast cooling condition was used.

Previously, Park et al.[9,10] reported the importance of suspended shapes of graphene at nano-terraces of the Cu surface in terms of relatively lower perturbation with the underlying Cu surface formed during the cooling process. This implies that a subtle difference in the nano-physical shape of graphene on nano-terraces of the Cu surface may be influential in determining the electrical properties. Moreover, a surface-enhanced Raman scattering (SERS) investigation of graphene with gap plasmon (Au nanoparticle-graphene-thin Au film) junctions has been carried out and experimentally confirmed the presence of significantly protruded domains of graphene along the z-direction, anticipating a negative influence on the electrical properties due to unwanted nano-physical

deformations[11-14] such as ripples.

On the basis of previous work, we focus on applying a new process technique to enhance the electrical properties of CVD grown graphene on the Cu surface intrinsically[15] and analyzing the details of deformed nano-physical shapes, ripples, of graphene on SiO_2/Si substrates after transfer.

3.2. Experimental section

3.2.1. Synthesis of graphene

Graphene films were synthesized on 25 μm thick copper foils through the CVD method, using methane (50 s.c.c.m.) and hydrogen (5 s.c.c.m.) gas with vacuum pumping (~1.5 mtorr) at 1000 。C for ~2 hours. Methane was used only during the growth stages of graphene and was not used during the cooling process.

3.2.2. Controlling the cooling rate

Controlling the cooling rate was carried out by adjusting the opening of the door of a furnace of a vertical type CVD chamber during the cooling process. For example, higher and lower cooling rates were simply controlled by opening the vertical chamber door fully and by ~5 cm, respectively. (Opening by ~20 cm was the intermediate cooling rate in this experiment.) The temperature was monitored by a thermocouple sensor inside the furnace. Although this temperature might be somewhat different from the temperature of the copper foil, the cooling rate would be more or less similar. We used the same copper foil from Nippon Mining (NM, Japan) and found that after 1000 °C annealing, they all have the (001) preferred orientation.

3.2.3. Fabrication of FET devices

Poly methyl methacrylate(PMMA) was spin-coated on top of graphene and the copper foil was etched in an ammonium persulfate solution (20 mM with distilled water). Highly p-doped Si substrates covered with 300 nm thick SiO_2 were used for the electrical measurement of graphene field effect transistor (GFET)devices. A free-standing graphene sheet on distilled water was carefully transferred onto a SiO_2/Si substrate, and PMMA was removed in acetone. Chromium (5 nm) and gold (30 nm) layers were deposited thermally for metal contacts of a 3-terminal graphene device with a pre-patterned stencil mask. Graphene channels of 230 μm width and 180 μm length were isolated through electron beam lithography.[16] 10 GFETs for each cooling rate were measured for enough statistics.

3.2.4. Characterization

Micro-Raman spectra were obtained using a 1 mW, 514 nm Ar-ion laser with a spot size of ~2 μm. (Renishaw inVia Raman Microscope.) The spectral resolution was about 1.6 cm^{-1}. An XE-100 (Park Systems) atomic force microscope (AFM) was used to obtain topography images. The measurements of GFETS were performed by using the three-terminal mode of an Agilent 2602 system applying a 10 mV source-drain voltage. The sheet resistance of the graphene sample (50 μm × 50 μm square geometry) was measured using a four-point probe with a nano-voltmeter (Keithley 6221/2182A).

3.3. Results and discussion

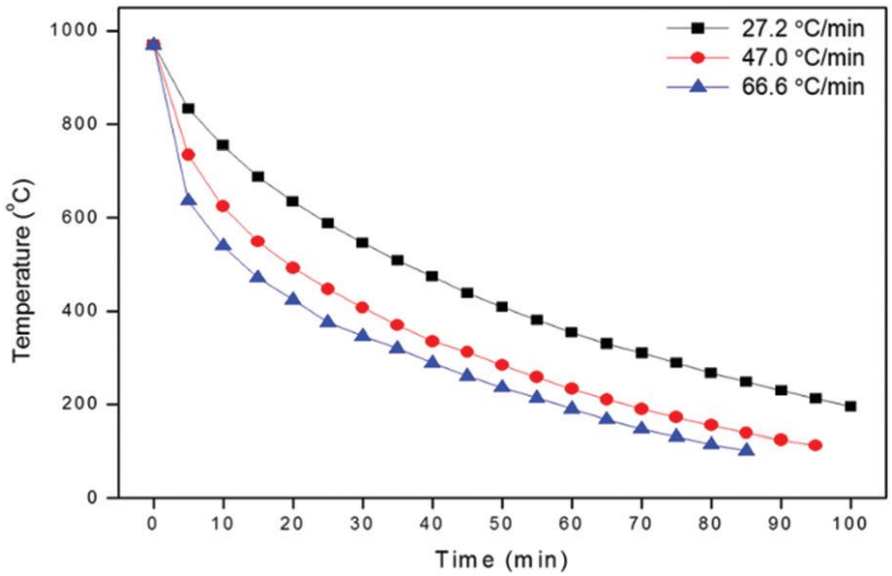

Figure. 3.1. Cooling rate profiles of CVD-grown graphene in this work. Note that the initial cooling rates are measured from the slopes during the first 5 min and are indicated in the legend.

Figure 3.1. shows the three different cooling rate profiles in this experiment (66.6, 47.0 and 27.2 $^{\circ}$C min^{-1}). It should be noted that the annealing temperature of all the samples are the same at ~1000。 C, and the cooling rates are measured from each profile during the first 5 min and indicated on the upper-right side of Fig. 3.1. Although this is not a very accurate estimate of the cooling rate, the characteristics of the graphene films exhibit definitive correlation with the estimated cooling rates. Although the graphene films are all grown and annealed at the same temperature of 1000 $^{\circ}$C, the difference in the cooling rate results in a significant difference in the morphology of the Cu substrate as well as that of the graphene films

after transfer onto SiO_2/Si substrates.

Figure 3.2.a–c show that the nano-terrace structure on the surface of Cu exhibits clear dependence on the cooling rate. Note that the morphology of the Cu surface should have been the same in all three cases because there was no difference in the growth parameters except for the cooling rate. During the cooling process, graphene expands due to a negative thermal expansion coefficient[17] whereas Cu contracts. If graphene remains conformal to the surface of Cu as many suspect, the difference in the thermal expansion coefficients would result in compressive strain on graphene after cooldown. If the strain is relieved by buckling of the graphene film, ripples would form. These ripples are in addition to the ripples due to the terrace structure of the Cu surface. A close inspection of the ripples on transferred graphene films in Figure 3.2.d–f reveals an interesting aspect. The red-colored numbers in Figure 3.2.b–e and c–f designate the distance measured between nano-terraces on the Cu surface and the ripple-to-ripple distances of graphene after transfer, respectively. If we define the "expansion ratio" as being the ratio of the ripple-to-ripple distances to the spacing between the nanoterraces on the Cu surface, this expansion ratio, on average, is larger than 1. This implies that not all terrace edges contribute to the ripples in transferred graphene and so the graphene film is not conformal to the Cu surface. Now, if we compare the expansion ratio for different cooling rates, we find a clear trend. It is 1.54 for 27.2 $^{\circ}C\ min^{-1}$ and 3.30 for 47.0 $^{\circ}C\ min^{-1}$. For 66.6 $^{\circ}C\ min^{-1}$, the ripple-to-ripple distance is not well defined, but the expansion ratio is clearly larger than 3.30. From these results, we argue that controlling the cooling rate may be a critical parameter in

determining the morphology of graphene before and after transfer.

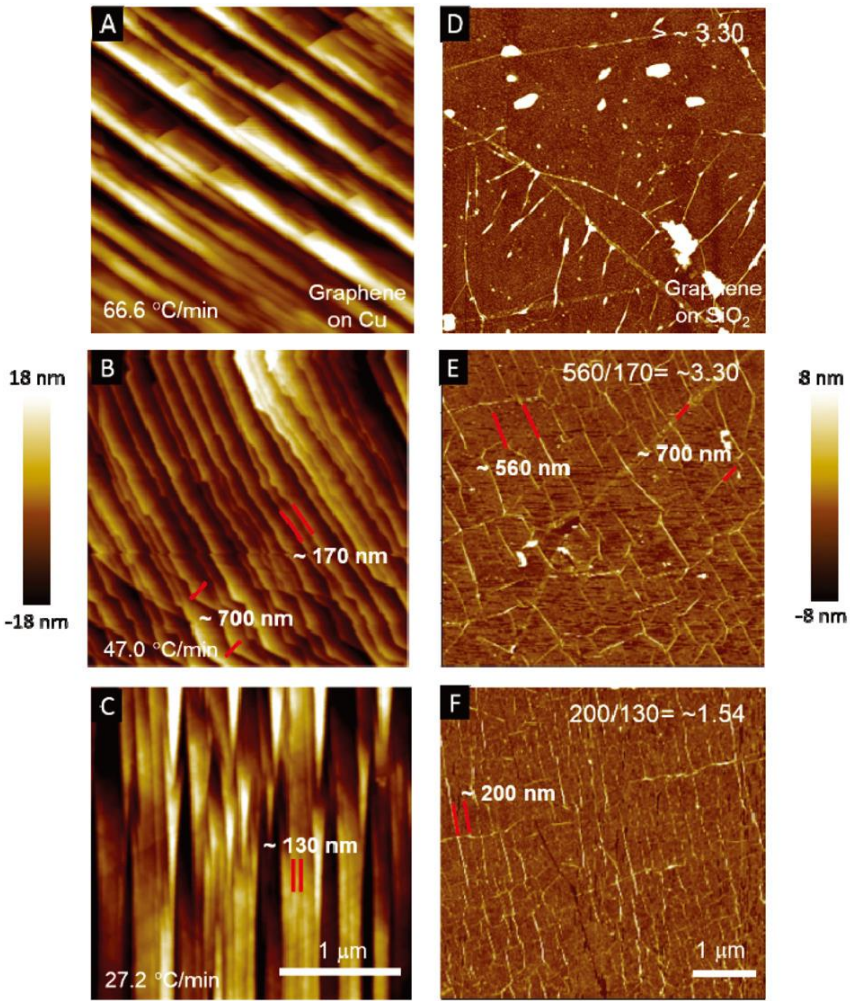

Figure 3.2. (a-c) Cu surface morphologies taken by AFM after graphene growth with different cooling rates. (66.6, 47.0 and 27.2 °C min^{-1}). (d-f)AFM images of graphene after transfer onto SiO_2/Si substrates. Representative distances between Cu nano-terraces and ripple-to-ripple distances on SiO_2/Si substrates are indicated in red. The expansion ratio values obtained by dividing the ripple-to-ripple distances on SiO_2/Si substrates by the distances between Cu nano-terraces are indicated in white.

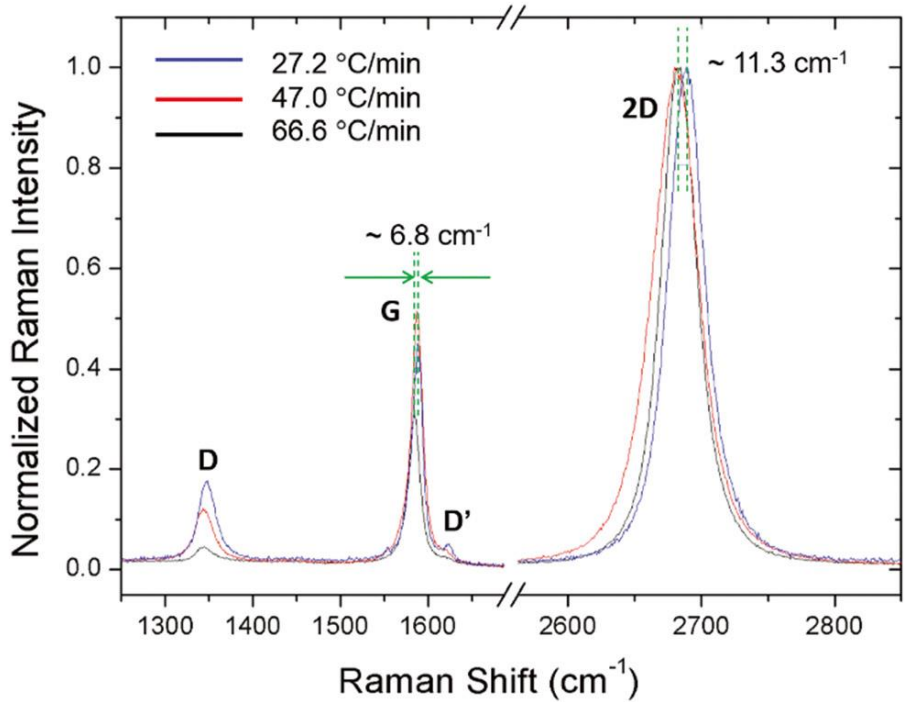

Figure 3.3. Representative Raman spectra for each cooling rate with band assignments. The relative peak shifts between the lowest cooling rate (blue) and the highest cooling rate (black) are indicated.

Figure 3.3. shows representative Raman spectra for the three cases taken after transfer. First, we can compare the contribution of sp^3 -type defects (D'/D value) for each cooling rate.[5] This ratio is the largest for the lower cooling rate (blue spectrum) and the smallest for the highest cooling rate. This is reasonable because some sp^3-type defects are associated with ripples. We should note that different cooling rates may affect recrystallization of graphene during the cooling process which would also affect the defect density. However, signals from such defects are not easy to separate from those from morphological defects such as ripples. Second, we turn our attention to the peak positions of the G and 2D bands. We notice

that both bands shift to a lower frequency for the higher cooling rate. It is well known that both doping and strain affect the peak positions, but the 2D band is less sensitive to doping than the G band,[18] whereas the 2D band is more sensitive to strain.[19] The fact that the 2D band is shifted more indicates that the major factor is strain. The relative redshifts of the G and 2D bands for the highest cooling rate indicate that the compressive strain is most relieved for the higher cooling rate.

Previously, Ni et al. reported that CVD graphene resulted in quasi-periodic nanoripple arrays (NRAs) and demonstrated that NRAs originated from Cu step edges. Such high-density NRAs, which are one of the serious steric obstacles in the surface morphology of graphene in terms of lateral carrier transport, give rise to flexural phonon scattering. Considering the scattering interaction between flexural phonons in NRA and electrons,[16,20–22] controlling NRAs is important for maximizing the lateral carrier mobility, and a new process to reduce NRAs during the CVD process is desirable. Here, we suggest that controlling the cooling rate offers a new way to reduce NRAs. Decreasing the ripple density and the resultant reduced flexural phonon–electron scattering can lead to enhanced electrical properties of graphene. In this work, we found that the lowest ripple density is obtained for the cooling rate of 66.6 $^{\circ}$C min^{-1}, and as anticipated, it leads to the best electrical properties.

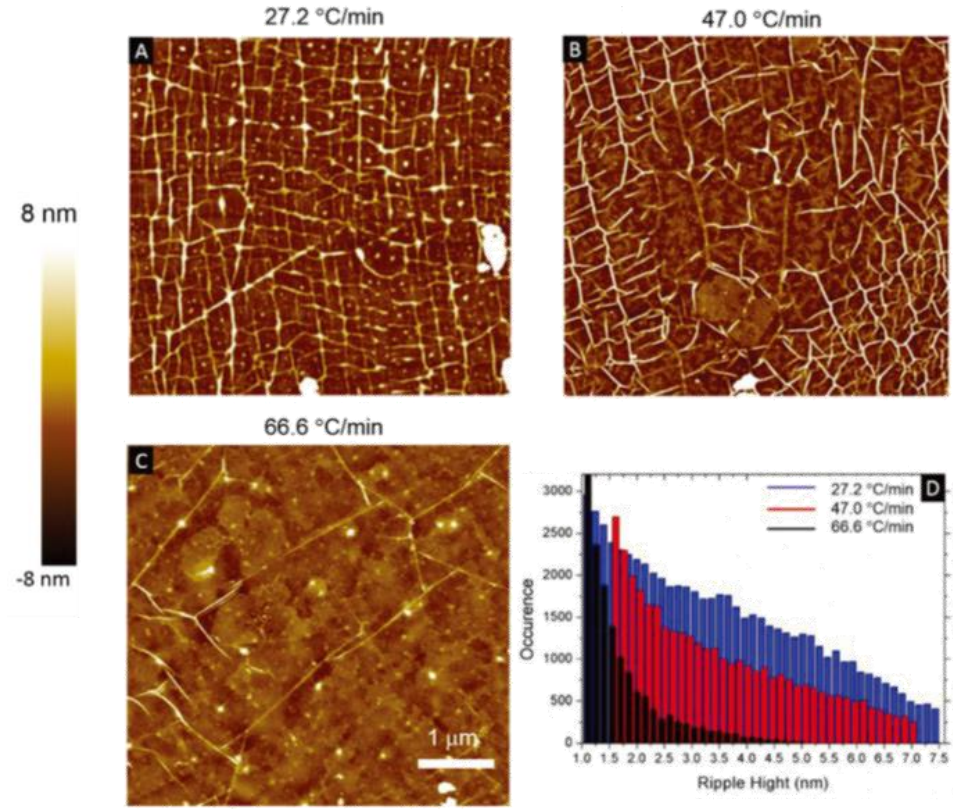

Figure 3.4. Representative (a-c) AFM images of graphene on the SiO_2/Si substrate deposited on a hydrophobic self-assembled monolayer. (d) Distribution of ripple heights for each cooling rate.

Next, we can compare the distribution of the ripple height for each cooling rate. Figure 3.4.a-c show the AFM images taken from graphene films prepared with cooling rates of 27.2 47.0 and 66.6 $^{\circ}C\ min^{-1}$, respectively. Figure 3.4.d shows overall ripple height distributions for these films. It shows that a higher cooling rate results in not only fewer ripples but also lower ripple heights. The influence of the cooling rate on the morphology further translates into an impact on the electrical properties.

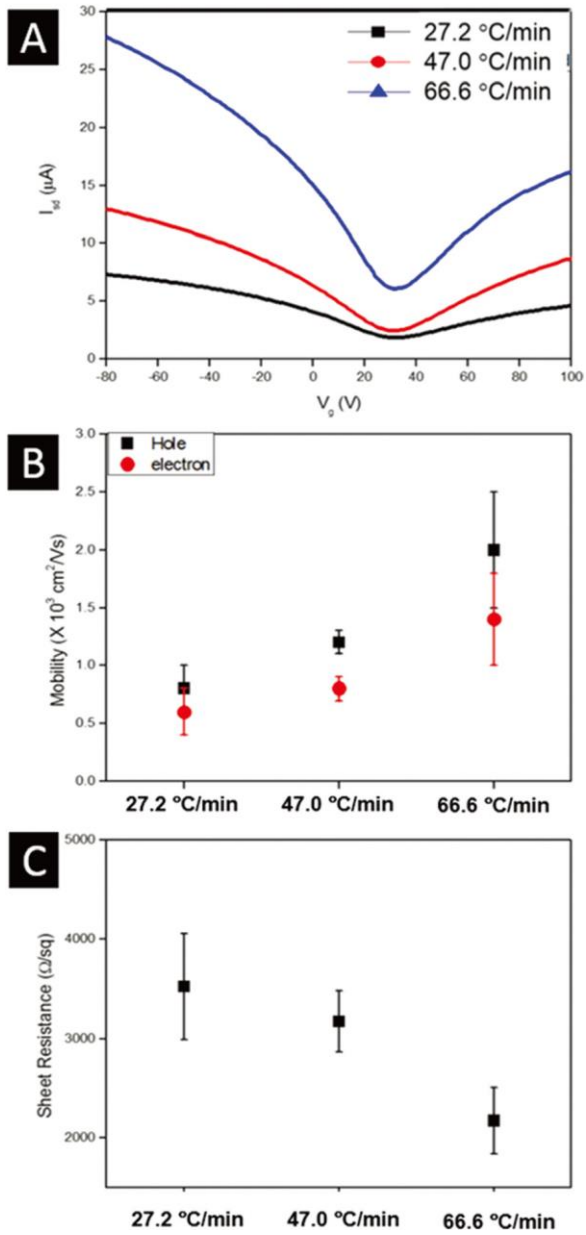

Figure 3.5. (a) Transferred *I/V* characteristic curves, (b) carrier mobility and (c) sheet resistance profile, for each cooling rate.

Figure 3.5.(a) displays the electrical characteristics of a GFET for each cooling rate. In order to avoid the substrate-induced doping effect, a hydrophobic self-assembled monolayer (SAMs) with alkyl chains is inserted between the graphene layer and the SiO_2/Si substrate.[23] As a result, GFETs constructed on SAMs with alkyl chains show higher electron/hole mobilities with lower Dirac point voltages. The obtained electron/hole mobilities for each cooling rate are shown in Figure 3.5.b. A higher cooling rate gives us higher electron/hole mobility values with nearly the same Dirac point voltages (~30 V). The same tendency is also revealed in R_s, although the overall absolute R_s values are somewhat high. (In this work, we focus on the trend with varying ripple densities and heights based on changing the cooling rate.) Based on these observations, we can claim that the reduced ripple density and heights obtained by a higher cooling rate have a beneficial impact of reducing the flexural phonon scattering effect and thus lead to high lateral carrier mobilities.

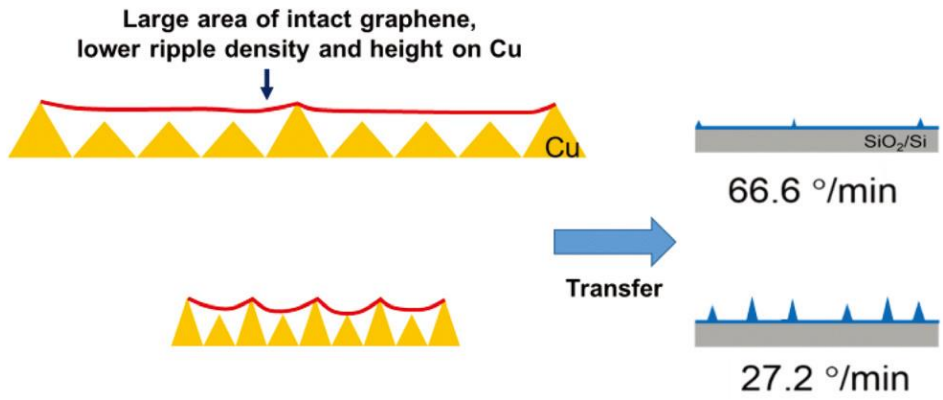

Figure 3.6. Overall schematic picture comparing two extreme cooling rates in this work.

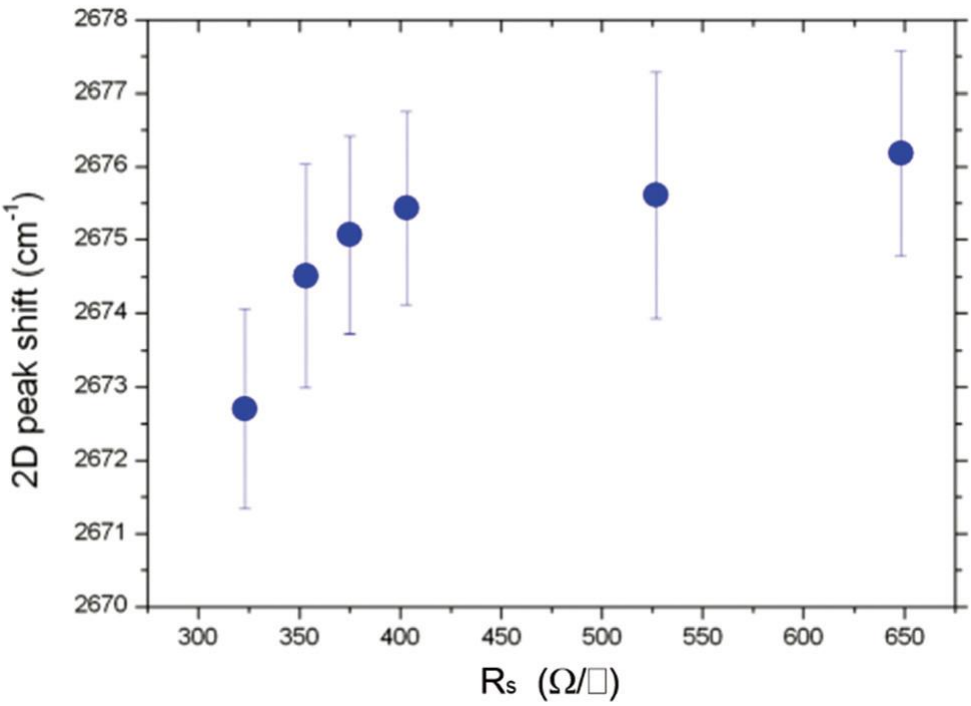

Figure 3.7. Correlation between the 2D-band peak shift of graphene on Cu and the R_s value measured after transferring onto a transparent flexible PET film.

A suggested mechanism for the enhanced electrical properties with a higher cooling rate is illustrated in Figure 3.6. Coarser nano-terrace formation for a higher cooling rate would result in fewer ripples even if each terrace edge contributes to the ripple formation. However, we observed that for higher cooling rates, fewer percentages of the terrace edges actually contribute to the ripple formation. This reduces the ripple density even further. This kind of configuration suggests that the graphene film is tauter for higher cooling rates, which has an effect of reducing the ripple heights after transfer as shown in Figure 3.6. Therefore, a subtle control of the nano-physical shape of graphene via modulating the cooling rate may be a good approach to fabricating electrically high quality graphene.

Park and colleagues previously reported the correlation between the 2D Raman peak shift of CVD-grown graphene on Cu and the R_s value after transfer onto polyethylene terephthalate (PET) films for flexible transparent electrodes.[8] A smaller shift of the 2D peak correlated with a lower R_s value implied that a specific hidden memory effect of graphene from the Cu surface to the PET substrate might be present as shown in Figure 3.7. However, the authors could not resolve the detailed mechanism of the memory effect at that time, and it remained a challenging issue. We can now unveil the relationship between the 2D peak shift and R_s based on the current investigation. We can infer that the 2D peak shift is derived from the mechanical strain on the Cu surface, which means that suspended and supported shapes of graphene are mixed according to the Cu surface morphology. Furthermore, the suspended graphene formation is very important in terms of less interference with the substrate. The degree of suspended graphene shape on Cu is affected by the

cooling rate and revealed via the red-shift of the 2D Raman peak. Upon employing different cooling rates, we can confirm that a higher suspended shape results from a higher expansion value and that the density of the ripples and their heights are reduced, which lead to improved electrical characteristics.

3.4. Conclusions

We suggest that by tuning the cooling rate one can control the electrical properties of CVD-grown graphene. A higher cooling rate gives rise to large suspended graphene formation during the cooling process, which in turn results in reduced ripple density and heights after transfer onto SiO_2/Si substrates. The correlation of the electron/hole mobilities and R_s with the cooling rate further substantiates the importance of controlling the cooling process, which may be useful also for graphene-based sensing applications based on subtle nano-physical deformation of graphene. Furthermore, we can also unveil the unresolved issue in previous work, in which transferred graphene with higher expansion on Cu can lead to a smaller ripple density and lower ripple heights after transfer, resulting in improved electrical characteristics.

3.5. References

1. A. K. Geim and K. S. Novoselov, The Rise of Grpahene. *Nat. Mater.* 2007, 6, 183.

2. K. S. Novoselov, A. K. Geim, S. V. Morozov, D. Jiang, Y. Zhang, S. V. Dubonos, I. V. Grigorieva and A. A. Firsov, Electric Field Effect in Atomically Thin Carbon Films. *Science* 2006, 306, 666.

3. X. Li, W. Cai, J. An, S. Kim, J. Nah, D. Yang, R. Piner, A. Velamakanni, I. Jung, E. Tutuc, S. K. Banerjee, L. Colombo and R. S. Ruoff, Large-Area Synthesis of High-Quality and Uniform Graphen Films on Copper Foils. *Science* 2009, 324, 1312.

4. S. Bae, H. Kim, Y. Lee, X. Xu, J.-S. Park, Y. Zheng, J. Balakrishnan, T. Lei, H. R. Kim, Y. I. Song, Y.-J. Kim, K. S. Kim, B. Oezyilmaz, J.-H. Ahn, B. H. Hong and S. Iijima, Roll-to-Roll Production of 30-Inch Graphene Films for Transparent Electrodes. *Nat. Nanotechnol.* 2010, 5, 574.

5. A. Eckmann, A. Felten, A. Mishchenko, L. Britnell, R. Krupke, K. S. Novoselov and C. Casiraghi, Probing the Nature of Defects in Graphene by Raman Spectroscopy. *Nano Lett.* 2012, 12, 3925.

6. M. S. Lee, K. Lee, S. Y. Kim, H. Lee, J. Park, K. H. Choi, H. Kim, H. K. Kim, D. G. Lee, S. Nam and J.-U. Park, High-Performance, Transparent, and Stretchable Electrodes Using Graphene-Metal Nanowire Hybrid Structures. *Nano Lett.* 2013, 13, 2814.

7. W.-H. Park, M. Jung, J.-S. Moon, W. Park, T. Kim, J. Lee, M. Joo and K. Park, Experimental Observation of a Suspended Single Layer Graphene Film on Cu Foil Grown via Chemical Vapor

Deposition Method. *Phys. Status Solidi B* 2013, 250, 1874.

8. W.-H. Park, M. Jung, J.-S. Moon, W. Park, T. Kim, J. Lee, M. Joo and K. Park, Experimental Confirmation of Suspended Few-Layered Graphene on a Cu Substrate Grown via the CVD Method and Correlated with the Electrical Performance on a PET Substrate *J. Phys. D: Appl. Phys.* 2013, 46, 345301.

9. W.-H. Park, Electrical performance of chemical vapor deposition graphene on PET substrate tailored by Cu foil surface morphology. *Eur. Phys. J.: Appl. Phys.* 2014, 67, 30701.

10. W.-H. Park, M. Jung, W. Park, J.-S. Moon, J. Lee, S. H. Noh, M. Joo, T. Kim and K. Park, Experimental Observation of Local Electrical Signature of Suspended Graphene Grown via Chemical Vapour Deposition Method. *J. Phys. D: Appl. Phys.* 2014, 47, 15306.

11. W.-H. Park, Quantification of the Relative z-Polarized Electromagnetic Field Contribution and Associated Investigation of Asymmetric Shape of Layer Breathing Mode from Au Nanoparticle–Graphene–Au Thin Film Junctions. *J. Phys. Chem. C* 2014, 118, 6989.

12. Y. H. Min and W.-H. Park, Exploring the Relative Bending of a CVD Graphene Monolayer with Gap-Plasmons. *Nanoscale* 2014, 6, 9763.

13. Y. H. Min and W.-H. Park, Experimental Identification of Tilted Bending Formation of Graphene Monolayer with Gap-Plasmon. *RSC Adv.* 2014, 4, 51966.

14. Y. Kim, J. Ryu, M. Park, E. S. Kim, J. M. Yoo, J. Park, J. H. Kang and B. H. Hong, A Highly Conducting Graphene Film with Dual-Side Molecular n-Doping. *ACS Nano* 2014, 8, 868.

15. D. S. Choi, K. S. Kim, H. Kim, Y. Kim, T. Kim, S.-H. Rhy, C.-M. Yang, D. H. Yoon and W. S. Yang, Effect of Cooling Condition on Chemical Vapor Deposition Synthesis of Graphene on Copper Catalyst. *ACS Appl. Mater. Interfaces* 2014, 6, 19574.

16. G.-X. Ni, Y. Zheng, S. Bae, H. R. Kim, A. Pachoud, Y. S. Kim, C.-L. Tan, D. Im, J.-H. Ahn, B. H. Hong and B. Oezyilmaz, Graphene-Ferroelectric Hybrid Structure for Flexible Transparent Electrodes. *ACS Nano* 2012, 6, 1158.

17. D. Yoon, Y. W. Son and H. Cheong, Negative Thermal Expansion Coefficient of Graphene Measured by Raman Spectroscopy. *Nano Lett.* 2011, 11, 3227.

18. A. Das, S. Pisana, B. Chakraborty, S. Piscanec, S. K. Saha, U. V. Waghmare, K. S. Novoselov, H. R. Krishnamurthy, A. K. Geim, A. C. Ferrari and A. K. Sood, Monitoring Dopants by Raman Scattering in an Electrochemically Top-Gated Graphene Transistor. *Nat. Nanotechnol.* 2008, 3, 210.

19. D. Yoon, Y. W. Son and H. Cheong, Strain-Dependent Splitting of the Double-Resonance Raman Scattering Band in Graphene. *Phys. Rev. Lett.* 2011, 106, 155502.

20. W. H. Lee, J. Park, Y. Kim, K. S. Kim, B. H. Hong and K. Cho, Control of Graphene Field-Effect Transistors by Interfacial Hydrophobic Self-Assembled Monolayers. *Adv. Mater.* 2011, 23, 3460.

21. S. V. Morozov, K. S. Novoselov, M. I. Katsnelson, F. Schedin, D. C. Elias, J. A. Jaszczak and A. K. Geim, *Phys. Rev. Lett.*, 2008, 100, 016602.

22. R. Kernera, G. G. Naumisb and W. A. Gómez-Arias, *Physica B*, 2012, 407, 2002.

23. A. Laitinen, M. Oksanen, A. Fay, D. Cox, M. Tomi, P. Virtanen and P. J. Hakonen, *Nano Lett.*, 2014, 14, 3009.

Chapter 4. Stable n-Type Doping of Graphene via High-Molecular-Weight Ethylene Amines

Parts of this chapter have been published in:

I. Jo, Y. Kim, J. Moon, S. Park, J. S. Moon, W. B. Park, J. S. Lee* and B. H. Hong*, *Phys. Chem. Chem. Phys.* 2015, 17, 29492.

4.1. Introduction

Graphene has been studied as one of the most fascinating 2D materials, which have potential to be adopted in optoelectronics or flexible electronics, and conducting electrodes owing to its unusual band structure and electrical tunability.[1, 2] The electrical behavior of graphene including work function, mobility, and sheet resistance is strongly affected by its interaction with the surroundings.[3, 4] Recently, studies to tune the electrical properties by engineering of interaction with surroundings have received significant attention. For example, controlling the atomic substitution,[5] molecular adsorption,[6] covalent functionalization,[7] dielectric substrate,[8] self-assembled monolayers under graphene,[9, 10] and the use of metallic thin films or nanoparticles[11] was investigated. However, covalent functionalization is unfavorable due to significant decrease in carrier mobility and conductivity, in spite of its advantage in stability. Compared to covalent doping, the non-covalent doping by chemical species is favored insignificant drop in carrier mobility, but

it also has an instability issue and weak doping strength, especially in n-dopants. It was reported a non-covalent and stable doping method.[12] However, experimental for structural effects are still lacking.

In this regard, a study that the dependence of molecular structure was investigated by selecting a series of ethylene amines (Sigma-Aldrich), including triethylenetetramine (TETA), tetraethylenepentamine (TEPA), pentaethylenehexamine (PEHA), and poly(ethyleneimine) (PEI), as a model system with various number of amine groups and dimension of molecules. These molecules have 4, 5, 6 (linear), and n (branched) amino groups, respectively, and their molecular structures are represented in Figure 4.1.a. In addition, the properties of each dopants are shown in Table 4.1. Our study suggests that the structure of chemical species determines the doping aspects in graphene.

Table 4.1. Comparing of three types of ethylene amines molecules.

	no. amines	molecular weight (g mol^{-1})	boiling point(°C)	vapor pressure at 20°C(Pa)
TETA	4	146	267	<1
TEPA	5	189	340	<1
PEHA	6	232	380	<1
PEI	n	~750,000	unknown	<1

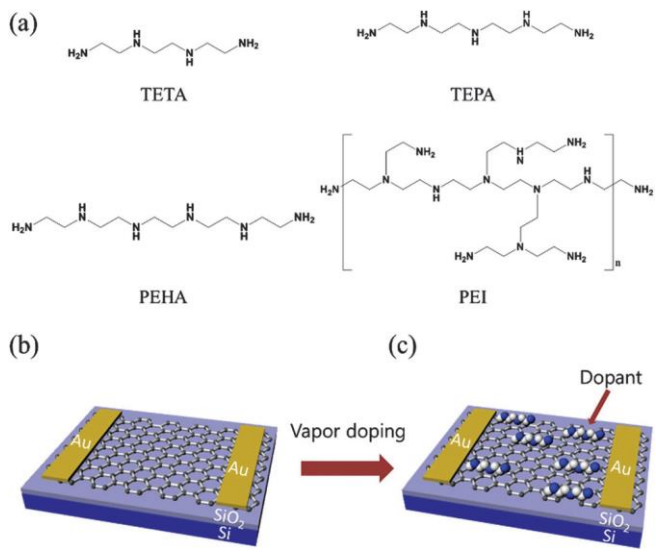

Figure 4.1. (a) Chemical structures of triethylenetetramine (TETA), tetraethylene pentaamine (TEPA), pentaethylenehexamine (PEHA), and poly(ethyleneimine) (PEI). Schematic diagram of the vapor-phase doping process (b) before and (c) after.

4.2. Experimental

Graphene samples used in this work were synthesized by low pressure chemical vapor deposition (LPCVD), described in the literature.[13, 14] The graphene film grown on copper foil was covered by poly(methylmethacrylate) (PMMA) and floated in a 0.1 M ammonium persulfate ($(NH_2)_4S_2O_8$) aqueous solution. The PMMA supported graphene film was transferred to the 300 nm SiO_2/p^+Si substrate after all the copper layers were etched away and rinsed in deionized water. Then, graphene field-effect transistors (FETs) were fabricated with Cr (5 nm) /Au (30 nm) source/drain electrodes to examine the electrical performance of doped graphene by different ethylene amines. Vapor-phase doping method, which shows more homogeneous doping than spin coating or dipping method, reported in the literature was used.[12] The target substrate with each dopant droplet was placed in a glass dish (Figure 4.1.b) and baked at 120°C for vaporizing molecule on the surface of graphene during 30 min (as shown in Figure 4.1.c and Figure 4.2.).

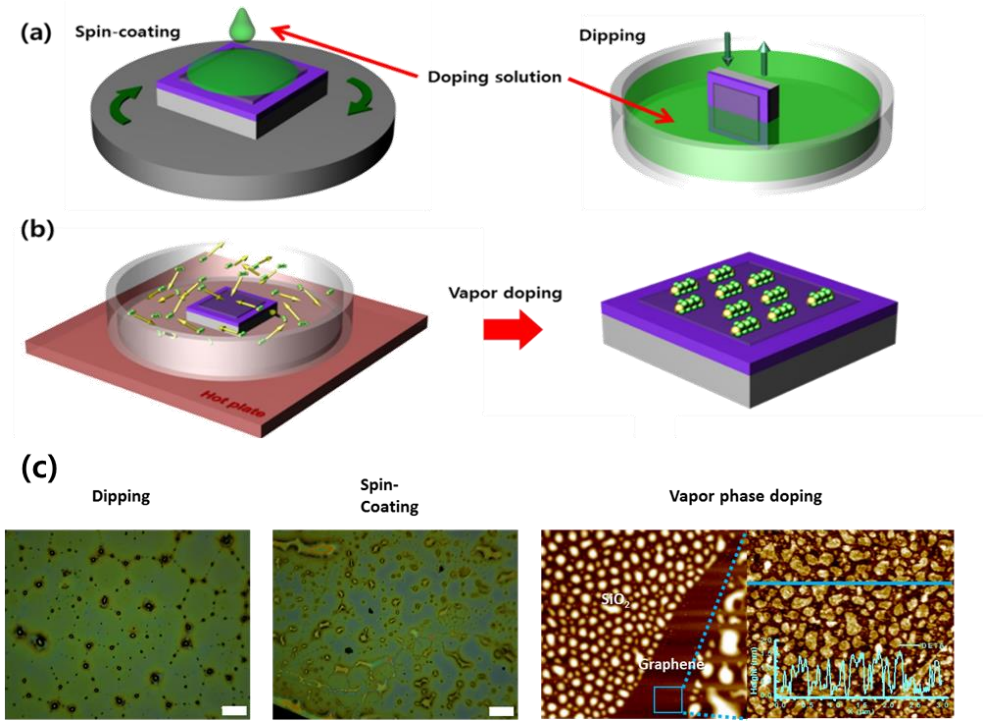

Figure 4.2. Schematic process of (a) spin-coating process (left), dipping (right), and (b) vapor phase doping. (c) Comparison of doping methods by optical microscope and AFM images. [Adapted from Ref. 12]

4.3. Results and Discussion

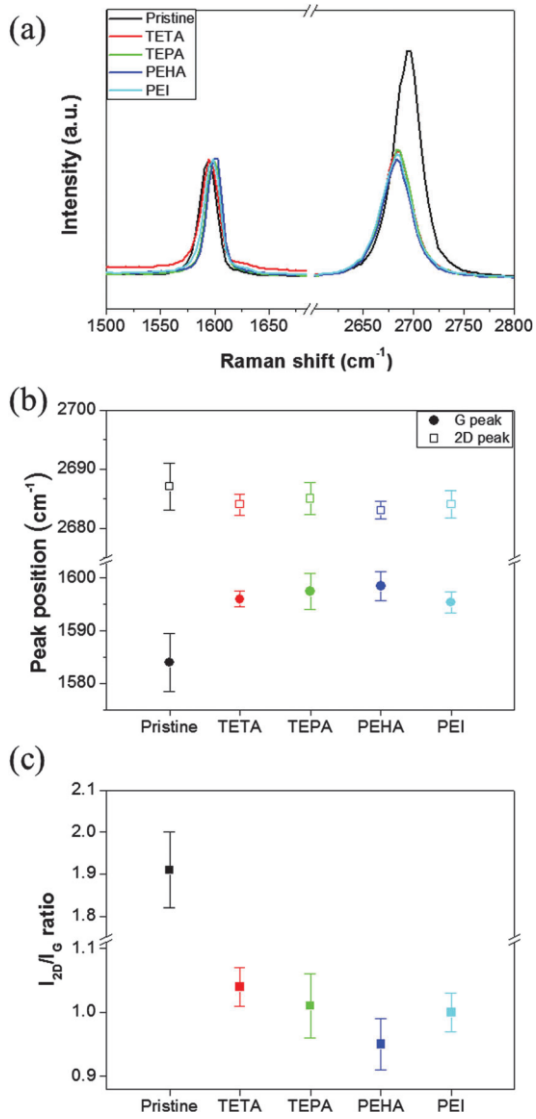

Figure 4.3. Raman spectra of graphene doped with different ethylene amines and peak parameter analysis: (a) Raman spectra obtained from the pristine graphene and the doped graphene, (b) G and 2D peak positions for the pristine graphene and the doped graphene, and (c) statistical ratio I_{2D}/I_G for pristine graphene and doped graphene.

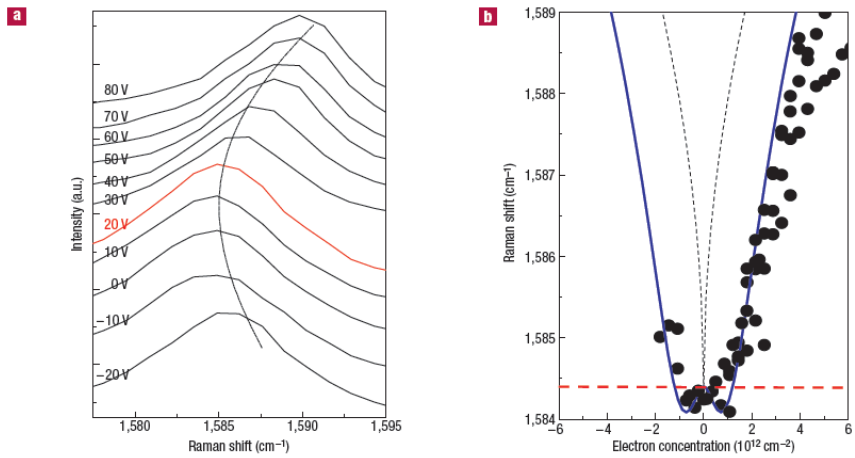

Figure 4.4. (a) Raman G peak of doped graphene. (b) G-peak position as a function of electron concentration. [Adapted from Ref. 18]

Raman spectroscopy is an ideal characterization tool for graphene research, which is used to determine the effects of perturbations, such as electric and magnetic fields, strain, and doping.[15] To characterize the ethylene amines doped graphene, we used 514 nm laser at room temperature with 10 mW power to reduce the damage during the measurement. Figure 4.3.a. shows the Raman spectra of the monolayer graphene and of the doped graphene with various ethylene amines, in which the typical Raman peaks of graphene, the G band (1584 cm^{-1}) and the 2D band (2700 cm^{-1}), are observed.[16] The G peak position of graphene was blue-shifted from 1583.7 cm^{-1} to 1595.3 cm^{-1} (TETA), 1596.1 cm^{-1} (TEPA), 1596.9 cm^{-1} (PEHA), and 1595.7 cm^{-1} (PEI) due to the effect of the Fermi level shift on the phonon frequencies as a result of electron doping.[17] The red-shift of 2D peak position is also observed, which indicate the increasing electron concentrations (Figure 4.3.b. and 4.4.).[18] These results indicate that ethylene amine doping is stronger as the number of

amino groups in the dopant increased (4, 5, and 6 for TETA, TEPA, and PEHA, respectively).[19, 20] However, the PEI-doped graphene shows a lower doping strength although numerous amino groups in PEI molecule.

Noticeably, the I_{2D}/I_G ratio that is used to estimate the doping intensity decreased after ethylene amine vapor-phase doping. The intensity ratio of 2D to G peak (I_{2D}/I_G) is used to estimate the doping intensity that represented to decrease with doping.[21] The ratio diminished from 1.93 for pristine graphene to 1.05, 1.02, 0.95, and 0.99 for TETA-, TEPA-, PEHA-, and PEI- doped graphene, respectively, shown in Figure 4.3.c. Raman features that changing the peak positions and the I_{2D}/I_G ratio confirm the stronger n-doping of linear ethylene amines as the number of amino groups increases. Thus, the amount of electrons injection per covered area is expected to increase with the number of amino groups. However, PEI-doped graphene shows a weaker n-doping effect, even though it has more amino groups than linear molecules. Thus, the n-doping of graphene is strongly related to the ethylene amine molecular structure.

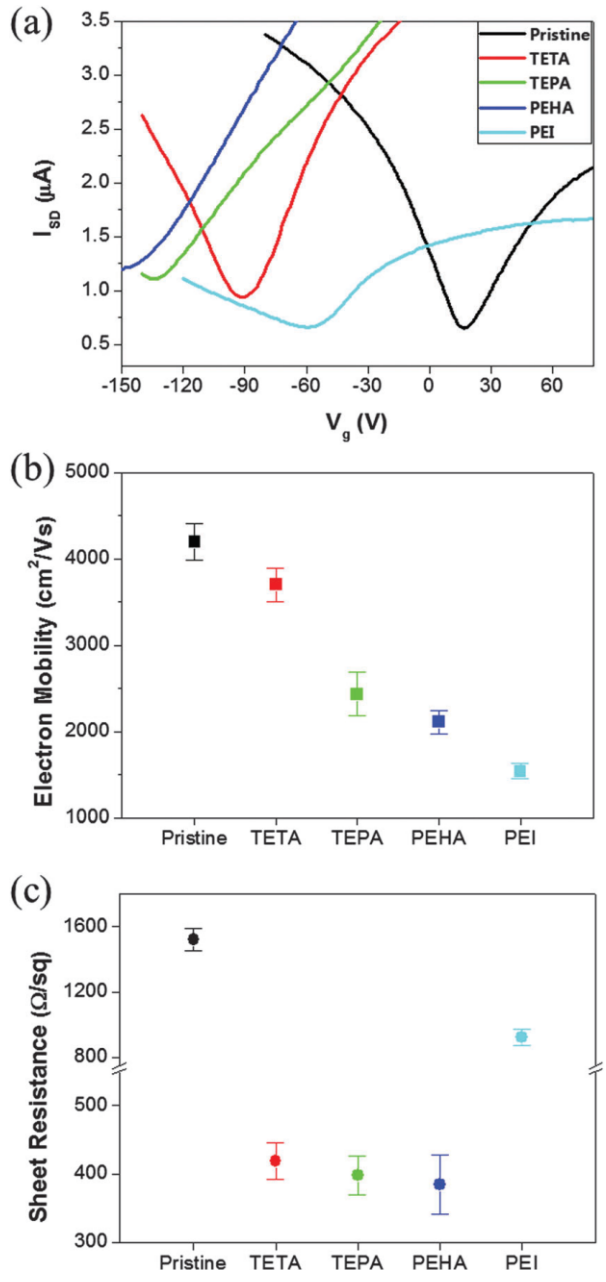

Figure 4.5. (a) Current-voltage transfer characteristics, (b) electron mobility, and (c) sheet resistance of pristine (black), TETA-doped (red), TEPA-doped (green), PEHA-doped (blue), and PEI-doped (cyan) graphene FET devices.

The electrical properties of a dozen of graphene transistors were measured to support the n-doping effects of ethylene amine dopants (Agilent 2602). The graphene transistors were fabricated by CVD graphene films grown from a single batch to avoid inconsistencies in graphene devices and doping processes. Fig. 3(a) shows the current-voltage characteristics of the back-gated pristine and of n-doped graphene FETs. At first, the Dirac voltage of the pristine graphene transistors was measured to be at 18 ± 5 V. The Dirac voltages were shifted to -94 ± 7 V, -135 ± 6 V, over -150 V, and -58 ± 7 V for TETA-, TEPA-, PEHA-, and PEI-doped graphene, respectively. In addition, the carrier concentrations were calculated to be 7.1×10^{12} for TETA doped graphene, 9.2×10^{12} for TEPA doped graphene, 1.01×10^{13} for PEHA doped graphene, and 4.9×10^{12} cm^{-2} for PEI-doped graphene by utilizing Eq. (2):[1, 21]

$$n = -\alpha(V_g - V_{CNP}) \qquad (1)$$

where $\alpha = 7.2 \times 10^{10}$ cm^{-2} V^{-1} and V_{CNP} is the charge neutral point voltage. These findings are consistent with the results obtained from the Raman analysis, implying that the charge transfer between molecules and graphene is maximized by increasing the functional groups in the linear dopant.

The mobility of each device was calculated in the linear regime,

using the Eq. (2):[8, 9]

$$I_D = \frac{WC_i}{L} V_D \mu (V_G - V_T) \quad (2)$$

where C_i = 1.08 × 10^{-8} F cm^{-2}, V_D = 0.01 V, W = 230 μm, and L = 180 μm. The estimated mobility of pristine graphene devices yields 4200 ± 210 cm^2 V^{-1} s^{-1} (hole region) and 4060 ± 178 cm^2 V^{-1} s^{-1} (electron region) that relatively high mobility for its scales. However, only the electron mobility of the doped graphene devices was compared, due to the lack of hole-region points. Doped graphene devices showed decreasing electron mobility as the number of amino groups increased. The electron mobility was measured to be 3700 ± 190, 2437 ± 250, 2110 ± 130, and 1540 ± 90 cm^2 V^{-1} s^{-1} for TETA-, TEPA-, PEHA-, and PEI-doped transistors, respectively. The results are plotted in Figure 4.4.b. To further clarify this doping characteristics, the sheet resistance of pristine and of doped graphene were measured on SiO_2 (300 nm)/Si substrates (Figure 4.4.c) with 4-terminal measurement with Van der Pauw geometry. The sheet resistance of pristine graphene gradually decreased from 1520.0 ± 67.6 Ω sq^{-1} to 418.6 ± 26.6 Ω sq^{-1}, 397.6 ± 28 Ω sq^{-1}, and 385.0 ± 43.4 Ω sq^{-1} for TETA-, TEPA-, and PEHA-doped graphene, respectively. However, PEI-doped graphene showed a high sheet resistance of 925.4 ± 49.0 Ω sq^{-1}, as PEI induced a lower doping effect on graphene. The electrical measurement results show the degradation of the mobility and the sheet resistance in doped graphene due to the amino functional groups acted as charge

impurities on graphene by the potential difference between pristine graphene and ethylene amines.[21]

The durability of doping is another issue in the fabrication of n-doped graphene devices. To compare the stability of doping for each dopants, the change of the Dirac voltage position and the sheet resistance with different ethylene amine doped graphene were all measured. Figure 4.5. depicts the changes with respect to the heating time in ambient conditions. Though doped graphene devices were heated during 20 min at 90°C, we obtained relatively stable Dirac voltage and sheet resistance as more functional groups in molecule, which changed under 50 Ω sq^{-1} of sheet resistance and 20 V at PEI-doped graphene, especially. This suggest that the stability of n-doping depends on the molecular size or the number of functional groups.

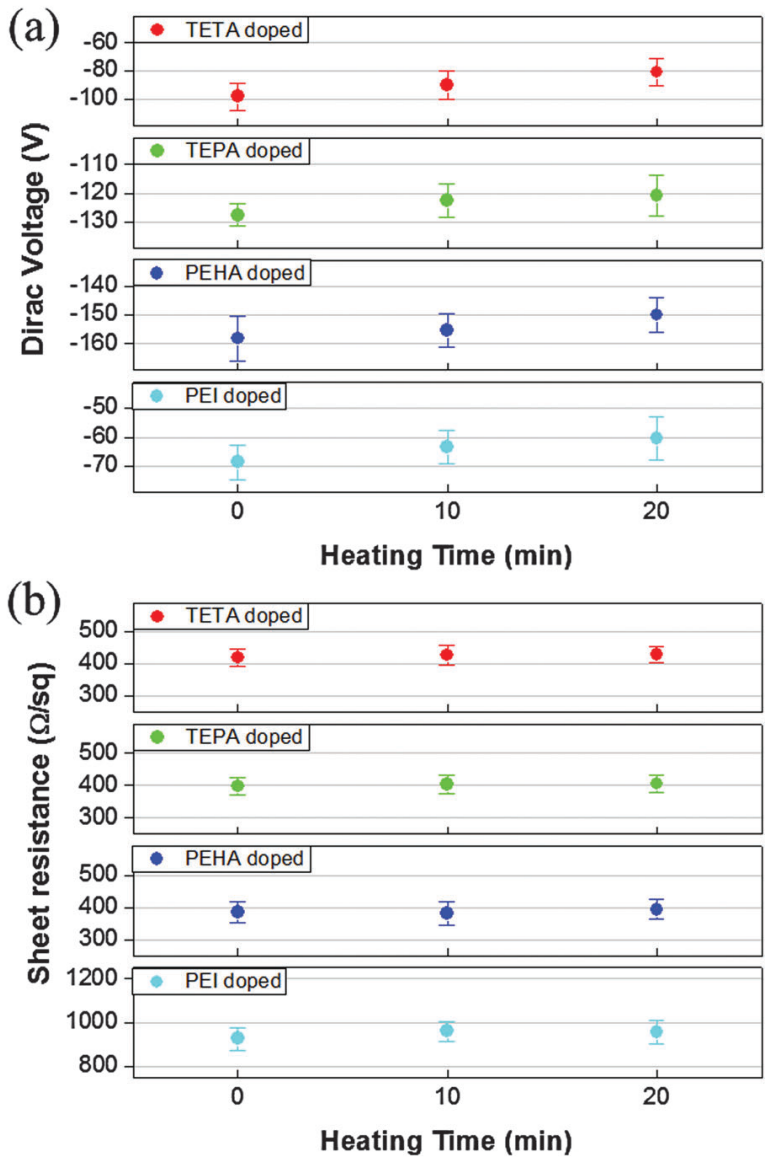

Figure 4.5. Changes in (a) Dirac voltage and (b) sheet resistance of TETA-doped (red), TEPA-doped (green), PEHA-doped (blue), and PEI-doped (cyan) graphene FETs with increasing annealing time at 90°C.

4.4. Conclusion

We have investigated the effect of the dopant structure and number of amines group in dopant by optically and electrically. The doping concentration was tuned as high as -1.01×10^{13} cm^{-2} and the sheet resistance was reduced down to 400 Ohm sq^{-1} by changing the number of functional group in molecules. The PEI, the branched ethylene amine structure, doped graphene shows weaker doping strength (~4.9×10^{12} cm^{-2}) and higher sheet resistance (~900 Ohm sq^{-1}) comparing to PEHA, although it has the most amino functional groups in the series of ethylene amine dopants. We suggest that these findings provide a basis for a better understanding of the structural effect of dopants, which can be used for the future exploiting of series of dopant.

4.5. References

1. K. S. Novoselov, A. K. Geim, S. V. Morozov, D. Jiang, Y. Zhang, S. V. Dubonos, I. V. Grigorieva and A. A. Firsov, Electric Field Effect in Atomically Thin Carbon Films *Science*, 2004, 306, 666.

2. Y. Zhang, Y.-W. Tan, H. L. Stromer and P. Kim, Experimental Observation of the Quantum Hall Effect and Berry's Phase in Graphene *Nature*, 2005, 438, 201.

3. A. H. Castro Neto, F. Guinea, N. M. R. Peres, K. S. Novoselov and A. K. Geim, The Electronic Properties of Graphene *Rev. Mod. Phys.*, 2009, 81, 109.

4. C. R. Dean, A. F. Young, I.Meric,C. Lee, L.Wang, S. Sorgenfrei, K.Watanabe, T. Taniguchi, P. Kim, K. L. Shepard and J.Hone, Boron Nitride Substrates for High-Quality Graphene Electronics *Nat. Nanotechnol.*, 2010, 5, 722.

5. D. C. Wei, Y. Q. Liu, Y. Wang, H. L. Zhang, L. P. Huang and G. Yu, Synthesis of N-doped Graphene by Chemical Vapor Deposition and its Electrical Properties *Nano Lett.*, 2009, 9, 1752.

6. S. Ryu, L, Liu, S. Berciaud, Y. J. Yu, H. Liu, P. Kim, G. W. Flynn, and L. E. Brus, Atmospheric Oxygen Binding and Hole Doping in Deformed Graphene on a SiO_2 Substrate *Nano Lett.*, 2010, 10, 4944.

7. M. Seifert, J. E. B. Vargas, M. Bobinger, M. Sachsenhauser, A. W. Cummings, S. Roche and J. A. Garrido, Role of Grain Boundaries in Tailoring Electronic Properties of Polycrystalline Graphene by Chemical Functionalization *2D Mater.*, 2015, 2, 024008.

8. Z. Hu, D. P. Sinha, J. U. Lee and M. Liehr, Substrate Dielectric Effects on Graphene Field Effect Transistors *J. Appl, Phys.*, 2014, 115, 194507.

9. J. Park, W. H. Lee, S. Huh, S. H. Sim, S. B. Kim, K. Cho, B. H. Hong, and K. S. Kim, Work-Function Engineering of Graphene Electrodes by Self-Assembled Monolayers for High-Performance Organic Field-Effect Transistors *J. Phys Chem. Lett.*, 2011, 2, 841.

10. Y. Kim, J. Park, J. Kang, J. M. Yoo, K. Choi, E. S. Kim, J.-B. Choi, C. Hwang, K. S. Novoselov and B. H. Hong, A Highly Conducting Graphene Film with Dual-Side Molecular n-Doping *Nanoscale,* 2014, 6, 9545.

11. K. Pi, K. M. McCreary, W. Bao, Wei Han, Y. F. Chiang, Yan Li, S.-W. Tsai, C. N. Lau, and R. K. Kawakami, Electronic Doping and Scattering by Transition Metals on Graphene *Phys. Rev. B*, 2009, 80, 075406.

12. S. Some, J. Kim, K. Lee, A. Kulkarni, Y. Yoon, S. Lee, T. Kim, and H. Lee, Highly Air-Stable Phosphorus-Doped n-Type Graphene Field Effect Transistors *Adv. Mater.*, 2012, 24, 5481.

13. Y. Kim, J. Ryu, M. Park, E. S. Kim, J. M. Yoo, J. Park, J. H. Kang and B. H. Hong, Vapor-Phase Molecular Doping of Graphene for High-Performance Transparent Electrodes *ACS Nano*, 2013, 8, 868.

14. X. Li, W. Cai, J. An, S. Kim, J. Nah, D. Yang, R. Piner, A. Velamakanni, I. Jung, E. Tutuc, S. K. Banerjee, L. Colombo, and R. S. Ruoff, Large-Area Synthesis of High-Quality and Uniform Graphene Films on Copper Foils *Science*, 2009, 324, 1312.

15. S. Bae, H. Kim, Y. Lee, X. Xu, J.-S. Park, Y. Zheng, J. Balakrishnan, T. Lei, H. R. Kim, Y. I. Song, Y.-J. Kim, K. S. Kim, B. Ozyilmaz, J.-H. Ahn, B. H. Hong, and S. Iijima, Roll-to-Roll Production of 30-inch Graphene Films for Transparent Electrodes *Nat. Nanotechnol.*, 2010, 5, 574.

16. A. C. Ferrari, D. M. Basko, Raman Spectroscopy as a Versatile Tool for Studying the Properties of Graphene *Nat. Nanotechnol.*, 2013, 8, 235.

17. A. C. Ferrari, J. C. Meyer, V. Scardaci, C. Casiraghi, M. Lazzeri, F. Mauri, S. Piscanec, D. Jiang, K. S. Novoselov, S. Roth, and A. K. Geim, Raman Spectrum of Graphene and Graphene Layers *Phys. Rev. Lett.*, 2006, 97, 187401.

18. S. Pisana, M. Lazzeri, C. Casiraghi, K. S. Novoselov, A. K. Geim, A. C. Ferrari, and F. Mauri, Breakdown of the adiabatic Born-Oppenheimer approximation in graphene *Nature Materials*, 2007, 6, 198.

19. A. Das, S. Pisana, B. Chakraborty, S. Piscanec, S. K. Saha, U. V. Waghmare, K. S. Novoselov, H. R. Krishnamurthy, A. K. Geim, A. C. Ferrari and A. K. Sood, Monitoring Dopants by Raman Scattering in an Electrochemically Top-Gated Graphene Transistor *Nat. Nanotechnol.*, 2008, 3, 210.

20. A. K. Geim and K. S. Novoselov, The Rise of Graphene *Nat. Mater.*, 2007, 6, 183.

21. T. Mohiuddin, A. Lombardo, R. Nair, A. Bonetti, G. Savini, R. Jalil, N. Bonini, D. Basko, C. Galiotis, N. Marzari, K. Novoselov, A. Geim, and A. Ferrari, Uniaxial Strain in Graphene by Raman

Spectroscopy: G Peak Splitting, Grüneisen Parameters, and Sample Orientation *Phys. Rev. B*, 2009, 79, 205433.

22. C. Casiraghi, S. Pisana1, K. S. Novoselov, A. K. Geim and A. C. Ferrari, Raman Fingerprint of Charged Impurities in Graphene *Appl. Phys. Lett.*, 2007, 91, 233108.

23. K. M. McCreary, K. Pi, A. G. Swartz, W. Han, W. Bao, C. N. Lau, F. Guinea, M. I. Katsnelson, and R. K. Kawakami, Effect of Cluster Formation on Graphene Mobility *Phys. Rev. B*, 2010, 81, 115453

24. A. Deshpande, C. H. Sham, J. M. P. Alaboson, J. M. Mullin, G. C. Schatz, and M. C. Hersam, Self-Assembly and Photopolymerization of Sub-2 nm One-Dimensional Organic Nanostructures on Graphene *J. Am. Chem. Soc.*, 2012, 134, 16759.

List of Publications

[1] S. Lee,† I. Jo,† S. Kang,† B. Jang, J. Moon, J. B. Park, S. Lee, S. Rho, Y. Kim and B. H. Hong* "Smart Contact Lenses with Graphene Coating for Electromagnetic Interference Shielding and Dehydration Protection", *ACS nano* (DOI: 10.1021/acsnano.7b00370)

[2] S. Uk, J. Moon, J. An, H.-Y. Ahn, D. J. Kim, I. Jo, C. Jeon, S. Han, B. H. Hong* and K. T. Nam* "Double-layer Graphene Outperforming Monolayer as Catalyst on Silicon Photocathode for Hydrogen Production", *ACS Appl. Mater. Interfaces* (DOI: 10.1021/acsami.6b11750)

[3] J. Kim, W.-G. Bae, S. Park, Y. J. Kim, I. Jo, S. Park, N. L. Jeon, W. Kwak, S. Cho, J. Park, H. N. Kim, K. S. Choi, H. Seonwoo, Y.-H. Choung, P.-H. Choung*, B. H. Hong* and J. H. Chung* "Engineering structures and functions of mesenchymal stem cells by suspended large-area graphene nanopatterns", *2D Materials* 2016, 3, 3.

[4] J. H. Kang, J. Moon, D. J. Kim, Y. Kim, I. Jo, C. Jeon, J. Lee* and B. H. Hong* "Strain relaxation of graphene layers by Cu surface roughening", *Nano Lett.* 2016, 16, 5993.

[5] B. Lee, J. H. Kang, I. Jo, D. Shin* and B. H. Hong* "Graphene-catalyzed photoreduction of dye molecules revealed by graphene enhanced Raman spectroscopy", *Phys. Chem. Chem. Phys.* 2016, 18, 3413.

[6] W.-H. Park,† I. Jo,† B. H. Hong* and H. Cheong* "Controlling the

ripple density and heights: a new way to improve the electrical performance of CVD-grown graphene", *Nanoscale* 2016, 8, 9822.

[7] I. Jo, Y. Kim, J. Moon, S. Park, J. S. Moon, W. B. Park, J. S. Lee* and B. H. Hong* "Stable n-type doping of graphene via high-molecular-weight ethylene amines", *Phys. Chem. Chem. Phys.* 2015, 17, 29492.

[8] Y. Park, S. Park, I. Jo, B. H. Hong* and Y. Hong* "Controlled growth of a graphene charge-floating gate for organic non-volatile memory transistors", *Organic Electronics* 2015, 27, 227.

[9] J. Moon, J. Park, C. Jeon, J. Lee, I. Jo, S.-H. Yu, S.-P. Cho, Y.-E. Sung* and B. H. Hong* "An electrochemical approach to graphene oxide coated sulfur for long cycle life", *Nanoscale* 2015, 7, 13249.

[10] S. Park, J. Park, I. Jo, S.-P. Cho, D. Sung, S. Ryu, M. Park, K.-A. Min, J. Kim, S. Hong, B. H. Hong* and B.-S. Kim* "In situ hybridization of carbon nanotubes with bacterial cellulose for three-dimensional hybrid bioscaffolds", *Biomaterials* 2015, 58, 93.

[11] T.-J. Lee, S. Park, S. H. Bhang, J.-K. Yoon, I. Jo, G.-J. Jeong, B. H. Hong* and B.-S. Kim* "Graphene enhances the cardiomyogenic differentiation of human embryonic stem cells", *Biochem. Biophy. Res. Co.* 2014, 452, 174.

초 록

그래핀의 발견은 재료 분야에 있어서 2차원 물질에 대한 새롭고 커다란 관심을 불러일으키는 계기를 마련하였다. 그래핀에 대한 관심으로 수많은 연구가 진행되었고, 그래핀의 처음 박리 이후 6년 만에 노벨물리학상이 수여될 정도였다. 하지만 그래핀은 높은 전하이동도 등 뛰어난 전기적 특성을 가짐에도 불구하고 밴드갭이 없기 때문에 전계효과트랜지스터와 같은 소자에 응용되기가 쉽지 않았다. 따라서 소자 응용을 위한 노력의 일환으로 그래핀의 밴드갭이 없는 문제를 해결하기 위해 외부 원자나 분자의 도핑, 탄소원자의 치환, 그래핀 모양의 기계적인 변형 등 지난 10여 년 간 수많은 노력을 기울여왔고 어느 정도 성과를 거두었다. 한편으로 그래핀의 발견은 지난 1960~70년대 주목받았던 다양한 층상구조 물질에 대한 새로운 관심을 불러일으켰고, 또한 그런 층상구조를 갖는 2차원 물질을 재조명하는 계기를 마련하였다.

하지만 이러한 재미있는 성질에도 불구하고 그 동안 대량합성법이 개발되지 못했기 때문에 실제 적용 가능한 기술에 대한 연구는 제한적이었다. 그에 따라 2차원 물질의 합성방법에 대한 연구가 많이 진행되어왔고 크게 top-down 방식과 bottom-up 방식이 있는데, top-down 방식인 기계적 박리법, 볼 밀링 방법, 그리고 화학적 박리 방법이 소개되고, bottom-up 방식에서는 화학기상증착 방법이 소개된다. 그 중에서도 CVD 방법이 그래핀의 이상적인 성질(기계적 박리법)에 가까우면서도 대량생산이 가능하다는 점에서 각광을 받고 있다. 그럼에도 불구하고 여전히 기계적 박리법과 비교하여 높은 면저항, 낮은 전하 이동도를 갖고 있다.

그래핀의 성질을 악화시키는 요소 중 한가지로는 CVD 그래핀의 성장시불규칙적인 핵 형성과 성장에서 나오는 다결정성과 그에 따른 그레인 바운더리가 있다. 또 다른 요소로는 CVD 공정 중에 필요한 냉각 공정에서 그래핀과 촉매기판과의 다른 열평창계수에 의해 생기는 주름이 있다.

이 논문은 구리 상에 CVD 법을 이용하여 성장시킨 그래핀에 관한 합

성 방법 및 특성 평가와 그 그래핀을 이용한 전계효과트랜지스터로의 응용에 관한 연구이다. 특히 합성 조건을 조절하여 면저항에서의 개선을 다루 었고. 또한 기상 증착 도핑을 이용하여 그래핀의 일함수를 조절하였다.

첫째로, 구리 촉매에 가하는 인장을 조절하여 그래핀을 성장시킨 연구에 관하여 다루었다. 이 방법은 인장 조절을 통해 구리 촉매의 결정성을 변화시켰으며 최적화된 구리 촉매를 통해 큰 그레인 사이즈와 높은 전하이동도를 가지는 그래핀을 성장시켰다.

둘째로, 냉각 속도를 조절함을 통해 CVD 그래핀의 전기적 성질들을 변화시킬 수 있음을 보였다. 빠른 냉각 속도는 그래핀이 구리와 약한 결합을 하여 웨이퍼 위로 전사하였을 때 적은 주름을 갖게 하여 주름에 의해 일어나는 전기적 성질 감소를 줄일 수 있었다.

마지막으로, 개선된 도핑 방법에 관한 연구를 다루었다. 도펀트의 구조와 도펀트 내의 아민 작용기의 개수에 따른 영향을 연구하였다. 도핑의 세기는 선형 구조의 에틸렌 아민 구조내에서 아민기의 개수가 증가할수록 세졌다. 하지만 비 선형 구조인 가지형 구조의 도펀트는 아민기가 많음에도 불구하고 약한 도핑 효과를 보였다.

이러한 연구는 미래에 그래핀 응용분야를 위한 대량 생산에 필요한 롤투롤 CVD 합성법을 통해 고 성능의 그래핀 합성에 중요한 아이디어를 제공할 수 있을 것이다.